

SILICA COATING OF MONODISPERSE HYDROPHOBIC MAGNETITE  
NANOPARTICLES THROUGH REVERSE MICROEMULSION  
TECHNIQUES

A THESIS SUBMITTED TO  
THE GRADUATE SCHOOL OF NATURAL AND APPLIED SCIENCES  
OF  
MIDDLE EAST TECHNICAL UNIVERSITY

BY

ZEYNEP ERGÜL

IN PARTIAL FULFILLMENT OF THE REQUIREMENTS  
FOR  
THE DEGREE OF MASTER OF SCIENCE  
IN  
MICRO AND NANOTECHNOLOGY

JANUARY 2012

Approval of the thesis:

**SILICA COATING OF MONODISPERSE HYDROPHOBIC MAGNETITE  
NANOPARTICLES THROUGH REVERSE MICROEMULSION  
TECHNIQUES**

submitted by **ZEYNEP ERGÜL** in partial fulfillment of the requirements for the degree  
of **Master of Science in Micro and Nanotechnology Department, Middle East  
Technical University** by,

Prof. Dr. Canan ÖZGEN  
Dean, Graduate School of **Natural and Applied Sciences**

\_\_\_\_\_

Prof. Dr. Mürvet VOLKAN  
Head of Department, **Micro and Nanotechnology Dept.**

\_\_\_\_\_

Prof. Dr. Mürvet VOLKAN  
Supervisor, **Chemistry Dept., METU**

\_\_\_\_\_

Prof. Dr. Necati Özkan  
Co-Supervisor, **Polymer Science and Technology Dept.,METU**

\_\_\_\_\_

**Examining Committee Members:**

Prof. Dr. O. Yavuz ATAMAN  
Chemistry Dept., METU

\_\_\_\_\_

Prof. Dr. Mürvet VOLKAN  
Chemistry Dept., METU

\_\_\_\_\_

Prof. Dr. Necati ÖZKAN  
Polymer Science and Technology Dept., METU

\_\_\_\_\_

Prof. Dr. Erdal BAYRAMLI  
Chemistry Dept., METU

\_\_\_\_\_

Prof. Dr. Macit ÖZENBAŞ  
Metallurgical and Materials Engineering Dept., METU

\_\_\_\_\_

**Date:**

09 /01 / 2012

**I hereby declare that all information in this document has been obtained and presented in accordance with academic rules and ethical conduct. I also declare that, as required by these rules and conduct, I have fully cited and referenced all material and results that are not original to this work.**

Name, Last Name : Zeynep ERGÜL

Signature :

## ABSTRACT

### SILICA COATING OF MONODISPERSE HYDROPHOBIC MAGNETITE NANOPARTICLES THROUGH REVERSE MICROEMULSION TECHNIQUES

ERGÜL, Zeynep

M.Sc., Department of Micro and Nanotechnology

Supervisor: Prof. Dr. Mürvet VOLKAN

Co-supervisor: Prof. Dr. Necati ÖZKAN

January 2012, 79 pages

Magnetic nanoparticles find broad applications in biomedical field such as drug delivery, hyperthermia and magnetic resonance imaging (MRI). For these applications magnetic nanoparticles need to be coated with suitable materials which are soluble, biocompatible and nontoxic. Among these materials, silica is the most often used coating material. This thesis is focused on preparation of silica coated iron oxide magnetic nanoparticles. Magnetic iron oxide nanoparticles are synthesized by thermal decomposition method. In the presence of iron acetylacetonate  $\text{Fe}(\text{acac})_3$ , a high boiling point organic solvent and a reducing agent, particle sizes ranging from about 5 nm to 7 nm were obtained. Nanoparticles were characterized by transmission electron microscopy (TEM).

The obtained nanoparticles were coated with ultra thin silica shell via reverse microemulsion method. The influence of the amount of Igepal CO-520,  $\text{NH}_4\text{OH}$  and TEOS was studied systematically and their amounts were optimized to yield monodisperse and well defined particles. The size of the silica coated magnetic

nanoparticles and their agglomerates were determined by TEM images and particle size analyzer (zeta sizer). X-Ray photoelectron spectroscopy (XPS) was used to confirm the presence of silica whenever the coating could not be seen by TEM measurements. Magnetic nanoparticles having 4-6 nm thickness of silica shell were obtained. The results showed that the amount of surfactant Igepal CO-520 played an important role in the reaction system.

**Keywords:** Magnetic Nanoparticles, Thermal decomposition method, Silica Coating, Reverse Microemulsion

## ÖZ

### MONODİSPERS HİDROFOBİK MANYETİK NANOPARÇACIKLARIN TERS MİKROEMÜLSİYON METODU İLE SİLİKA KAPLANMASI

ERGÜL, Zeynep

Yüksek Lisans, Mikro ve Nanoteknoloji Bölümü

Tez Yöneticisi: Prof. Dr. Mürvet VOLKAN

Ortak Tez Yöneticisi: Prof. Dr. Necati ÖZKAN

Aralık 2011, 79 sayfa

Manyetik nanoparçacıklar yaygın olarak ilaç taşınımı, hipertermi ve manyetik rezonans görüntüleme (MR) alanlarında kullanılmaktadır. Bu uygulamalar için, manyetik nanoparçacıklarının çözünebilir, biyo-uyumlu ve toksik-olmayan uygun malzemeler ile kaplanması gerekmektedir. Bu malzemeler içerisinde, silika en çok kullanılan kaplama malzemesidir. Bu tezde, silika kaplı manyetik nanoparçacıklar üzerine odaklanılmıştır. Manyetik demir oksit nanoparçacıkları, yüksek sıcaklıkla parçalanma yöntemi ile sentezlenmiştir. Demir asetilasetonat  $Fe(acac)_3$ , kaynama noktası yüksek organik bir çözücü ve bir indirgen varlığında, boyutları 5- 7 nm arasında olan parçacıklar elde edilmiştir. Nanoparçacıklar geçirimli elektron mikroskobu (TEM) ile karakterize edilmiştir.

Elde edilen nanoparçacıklar, ters mikroemülsiyon yöntemi ile ultra ince silika kabuk ile kaplanmıştır. Igepal CO-520,  $NH_3(aq)$  and TEOS miktarlarının etkisi sistematik olarak çalışılmış ve miktarları, monodispers ve iyi dağılmış parçacıklar elde etmek için optimize edilmiştir. Silika kaplı manyetik nanoparçacıklarının boyutları ve aglomeratlarının karakterizasyonu TEM görüntüleri, parçacık boyut analizi (zeta sizer) ile yapılmıştır. TEM ölçümlerinde görüntülenemeyen

silikaların varlığını doğrulamak için X-ışını Fotoelektron Spektroskopisi (XPS) kullanıldı. Elde edilen sonuçlara göre, yüzey aktif madde olarak kullanılan Igepal CO-520, reaksiyon sisteminde önemli bir rol almış olup, 4-6 nm boyutlarında ince kabuk ile kaplanmış silika kaplı manyetik nanoparçacıklar elde edilmiştir.

Anahtar Kelimeler: Manyetik Nanoparçacıklar, Yüksek Sıcaklıkta Parçalanma Metodu, Silika Kaplama, Ters Mikroemülsiyon Metodu

**To my Parents**



## ACKNOWLEDGEMENTS

I am heartily thankful to my supervisor, Prof. Dr. Mürvet Volkan, whose encouragement, guidance and support from the initial to the final level enabled me to develop an understanding of the subject.

I would like to thank my co-supervisor, Prof. Dr. Necati Özkan for his guidance and valuable suggestions during this study.

Special thanks to Tuğba Nur Aslan, not only she helped me so much during my study but also she gave me moral support and warm friendship.

I would like to thank Dr. Murat Kaya for his guidance and support.

I would like to thank Yeliz Akpınar, Ceren Uzun and Dilek Ünal for their continuous help during my study. Thank them so much for everything.

I would like to thank Gülfem Aygar for her great friendship. I am very lucky to convince her to join this lab with me.

I would like to thank Elif Kanbertay, Zehra Tatlıcı, Bahar Köksal, Ufuk Özgen, Üzeyir Doğan, and all C50 lab members for their help and friendship. Thanks to them I never felt alone during this study.

I would like to thank Dr. Elif Tarhan Bor during this study. She helped me so much during TEM measurement measurements in Central Laboratory and also she gave me support and friendship.

Huge thanks to Deniz Tuncer, for her friendship, love and support. I am very lucky to have such a good friend, whenever I laugh, whenever I cry and whenever I need her, she was always with me.

Endless thank to my family, Berna Ergül, Aziz Ergül and Tunç Ergül for their love, trust and patience. They gave me endless love, believe me and support me every situation.

Lastly, I would like to thank my love, Emre Yılmaz. Without him, I will not have the courage and the chance to reach an end for this study. Thank you for your endless love, support, trust and patience.

## TABLE OF CONTENTS

ABSTRACT.....	iv
ÖZ .....	vi
ACKNOWLEDGEMENTS .....	ix
TABLE OF CONTENTS.....	xi
LIST OF TABLES .....	xiv
LIST OF FIGURES .....	xv
1. INTRODUCTION.....	1
1.1 Nanotechnology and Nanoparticles .....	1
1.2 Magnetic Nanoparticles .....	4
1.3 Applications of Magnetic Nanoparticles.....	5
1.4 Iron Oxide Magnetic Nanoparticles .....	6
1.4.1 Maghemite.....	8
1.4.2 Magnetite.....	8
1.5 Magnetism and Magnetic Properties.....	9
1.5.1 Diamagnetism .....	9
1.5.2 Paramagnetism .....	10
1.5.3 Ferromagnetism and Ferrimagnetism .....	11
1.5.4 Antiferromagnetism .....	12
1.5.5 Superparamagnetism .....	13
1.6 Synthesis of Iron Oxide Magnetic Nanoparticles .....	15
1.6.1 Thermal Decomposition Method .....	16
1.7 Surface Modification of Iron Oxide Magnetic Nanoparticles.....	17
1.8 Sol-Gel Process .....	19
1.9 Microemulsion .....	20
1.9.1 Silica Coating Through Inverse Microemulsion.....	22
1.10 Aim of the Study .....	25
2. EXPERIMENTAL .....	26

2.1 Chemicals and Reagents .....	26
2.1.1 Synthesis of Iron Oxide Nanoparticles .....	26
The following chemicals and materials were used for the syhthesis of iron oxide nanoparticles by Thermal Decomposition Method 1 .....	26
The following chemicals and materials were used for the syhthesis of iron oxide nanoparticles by Thermal Decomposition Method 2 .....	27
The following chemicals and materials were used for the Silica Coating on Iron Oxide Nanoparticles by Reverse Microemulsion Method .....	27
2.2 Instrumentation .....	28
2.2.1 Centrifuge.....	28
2.2.2 Transmission Electron Microscope (TEM).....	28
2.2.3 X-Ray Photoelectron Spectroscopy (XPS) .....	29
2.2.4 Particle Size Analyzer (Zeta Sizer).....	29
2.3 Procedure .....	29
2.3.1 Synthesis of Iron Oxide Nanoparticles by Thermal Decomposition Method 1 .....	29
2.3.2 Synthesis of Iron Oxide Nanoparticles by Thermal Decomposition Method 2 .....	31
2.3.3 Silica Coating on Iron Oxide Nanoparticles by Reverse Microemulsion Method .....	32
3. RESULTS AND DISCUSSION .....	34
3.1 Synthesis of Iron Oxide Nanoparticles by Thermal Decomposition Method .....	34
3.1.1 Magnetic Properties of Synthesized Magnetite Nanoparticles .....	43
3.2 Silica Coating on Iron Oxide Nanoparticles by Reverse Microemulsion Method .....	44
3.2.1 Effect of Surfactant on the Silica Coated Iron Oxide Nanoparticles (IGEPAL CO-520).....	48
3.2.2 Effect of TEOS Solution on Silica Coated Iron Oxide Nanoparticles .	59
3.2.3 Effect of Ammonia Solution on Silica Coated Iron Oxide Nanoparticles .....	63

4. CONCLUSIONS.....	71
---------------------	----

## LIST OF TABLES

### TABLES

<b>Table 1</b> Some Materials in Nanometers [4].....	3
<b>Table 2</b> Comparison of the synthetic methods [10].....	15
<b>Table 3</b> The Polydispersivity index values from the DLS method versus particle homogeneity.....	48
<b>Table 4</b> Various surfactant (Igepal CO-520) concentrations used for the synthesis of silica coated iron oxide nanoparticles at low TEOS concentration. ....	49
<b>Table 5</b> Various surfactant (Igepal CO-520) concentrations used .....	54
<b>Table 6</b> Various concentrations of TEOS used for the preparation of silica coated iron oxide particles.....	59
<b>Table 7</b> Various concentrations of $\text{NH}_3(\text{aq})$ used for the preparation of silica coated iron oxide particles at low TEOS concentration.....	64
<b>Table 8</b> Various $\text{NH}_3(\text{aq})$ concentrations used for the synthesis.....	69

## LIST OF FIGURES

### FIGURES

<b>Figure 1</b> This is a reference to what Feynman has said: “there is plenty of space at the bottom” and also to the failure of the “biotechnology age “in delivering what it promised.....	1
<b>Figure 2</b> Schematic of magnetic nanoparticles applications, (a) through the Drug Delivery Systems (DDS) functionalized MNP build up in the tumor tissue, (b) as a diagnosis tool for cancer by magnetic resonance imaging (MRI) or for magneto impedance (MI) sensor, (c) as a hyperthermia treatment for cancer [20].....	6
<b>Figure 3</b> Chemical formula for the magnetite/maghemite system[12]. .....	8
<b>Figure 4</b> Diamagnetism .....	10
<b>Figure 5</b> Paramagnetism.....	11
<b>Figure 6</b> Ferromagnetism .....	12
<b>Figure 7</b> The magnetic moment of single-domain superparamagnetic NPs aligns with the applied field. Superparamagnetic NPs will exhibit no net magnetization due to rapid reversal of magnetic moment [45]. .....	14
<b>Figure 8</b> Sol gel general reaction mechanism .....	19
<b>Figure 9</b> Schematic representation of a) oil-in-water microemulsion,.....	21
<b>Figure 10</b> Scheme of the two possible mechanism for silica growth on quantum dots [76]. .....	23
<b>Figure 11</b> Scheme of the mechanism for the formation of iron oxide core-silica shell nanoparticles [78]. .....	24
<b>Figure 12</b> Scheme for synthesis of Fe <sub>3</sub> O <sub>4</sub> nanoparticles.....	30
<b>Figure 13</b> Experimental setup for the synthesis of magnetic iron oxide nanoparticles with Thermal Decomposition Method.....	30
<b>Figure 14</b> The synthesis of magnetite nanoparticles .....	31
<b>Figure 16</b> Microemulsion system was formed. ....	32
<b>Figure 17</b> Magnetic separation; a magnet is attached to the container wall of a solution of SiO <sub>2</sub> - Fe <sub>3</sub> O <sub>4</sub> nanoparticles (•) and acetone (◊).....	33

<b>Figure 18</b> Synthesis of iron oxide nanoparticles a) Method 2, b) Method 1 .....	36
<b>Figure 19</b> Picture of a) heavily agglomerated iron oxide particles using 15 cm-column b) Stable suspension of the iron oxide nanoparticles using 25 cm-column .....	37
<b>Figure 20</b> TEM images of iron oxide nanoparticles synthesized by Thermal Decomposition Method 2 at three different magnification. Iron Precursor: Fe(acac) <sub>3</sub> , solvent: benzyl ether, reducing agent: Oleylamine.....	39
<b>Figure 21</b> TEM images of iron oxide nanoparticles synthesized by thermal decomposition Method 2.....	40
<b>Figure 22</b> TEM images of iron oxide nanoparticles synthesized by Thermal Decomposition Method 1. Iron Precursor: Fe(acac) <sub>3</sub> , solvent: benzyl ether, reducing agent: 1,2-hexadecanediol. Reflux time was 60 min. instead of 30 min	41
<b>Figure 23</b> TEM image of iron oxide nanoparticles synthesized by thermal decomposition method 2 washed once with ethanol.....	42
<b>Figure 24</b> The behavior of the iron oxide nanoparticles dispersed in hexane under an external magnetic field (1.6 T) applied. a) the stable suspension of iron oxide particles b) large agglomerates of iron oxide particles. ....	43
<b>Figure 25</b> Chemical formula of Igepal CO-520 .....	45
<b>Figure 26</b> Synthesis of Silica Coated Iron Oxide Nanoparticles.....	46
<b>Figure 27</b> Reference solution (Prepared by diluting 467 μl iron oxide nanoparticles to 10 ml cyclohexane).....	47
<b>Figure 28</b> Photographs of iron oxide nanoparticles following silica coating process. Various amounts of Igepal CO-520 were used at low TEOS concentration, batches A-E a) 500 μl Igepal CO-520; batch A, b) 1000 μl Igepal CO-520; batch B c) 1200 μl Igepal CO-520; batch C d) 1300 μl Igepal CO-520; batch D e) 1500 μl Igepal CO-520; batch E, (80 μl TEOS was used).....	50
<b>Figure 29</b> TEM images of the silica coated iron oxide nanoparticles prepared using 80 μl TEOS, 150 μl NH <sub>3</sub> (aq) and Igepal CO-520 a) 1000 μl Igepal CO-520; batch B, b) 1300 μl Igepal CO-520; batch D. ....	51
<b>Figure 30</b> XPS result of silica coated iron oxide nanoparticles of batch B.....	52



<b>Figure 31</b> The agglomerate size distribution of the silica coated iron oxide nanoparticles prepared using 1000 $\mu\text{l}$ Igepal CO-520, 80 $\mu\text{l}$ TEOS and 150 $\mu\text{l}$ of $\text{NH}_3(\text{aq})$ .....	53
<b>Figure 32</b> Photographs of iron oxide nanoparticles following silica coating process. Various amounts of Igepal CO-520 were used at high TEOS concentration, batches A-D a) 500 $\mu\text{l}$ Igepal CO-520; batch A, b) 1000 $\mu\text{l}$ Igepal CO-520; batch B c) 1300 $\mu\text{l}$ Igepal CO-520; batch C d) 1500 $\mu\text{l}$ Igepal CO-520; batch D (100 $\mu\text{l}$ TEOS was used).....	55
<b>Figure 33</b> TEM images of iron oxide nanoparticles following silica coating process. Various amounts of Igepal CO-520 were used at high TEOS concentration and 150 $\mu\text{l}$ $\text{NH}_3(\text{aq})$ a) 1300 $\mu\text{l}$ Igepal CO-520; batch C b) 1500 $\mu\text{l}$ Igepal CO-520; batch D. (100 $\mu\text{l}$ TEOS was used).....	56
<b>Figure 34</b> The agglomerate size distribution of the silica coated iron oxide nanoparticles prepared using 1300 $\mu\text{l}$ Igepal CO-520, 100 $\mu\text{l}$ TEOS and 150 $\mu\text{l}$ of $\text{NH}_3(\text{aq})$ . .....	58
<b>Figure 35</b> Photographs of iron oxide nanoparticles following the silica coating process in which various amounts of TEOS were used. a) 60 $\mu\text{l}$ TEOS; batch A, b) 70 $\mu\text{l}$ TEOS; batch B c) 80 $\mu\text{l}$ TEOS; batch C d) 100 $\mu\text{l}$ TEOS; batch D e) 120 $\mu\text{l}$ TEOS; batch E. Volume of Igepal CO-520 was 1300 $\mu\text{l}$ . .....	60
<b>Figure 36</b> TEM images of the silica coated iron oxide nanoparticles prepared using 1300 $\mu\text{l}$ Igepal CO-520 and various amounts of TEOS a) 80 $\mu\text{l}$ TEOS; batch C, b) 100 $\mu\text{l}$ TEOS; batch D was used. ....	61
<b>Figure 37</b> The agglomerate size distribution of the silica coated iron oxide nanoparticles prepared using 1300 $\mu\text{l}$ Igepal CO-520, 120 $\mu\text{l}$ TEOS and 150 $\mu\text{l}$ of $\text{NH}_3(\text{aq})$ , batch E. ....	62
<b>Figure 38</b> Photographs of iron oxide nanoparticles following the silica coating process in which various amounts of $\text{NH}_4\text{OH}$ a) 75 $\mu\text{l}$ $\text{NH}_4\text{OH}$ ; batch A b) 100 $\mu\text{l}$ $\text{NH}_4\text{OH}$ ; batch B c) 150 $\mu\text{l}$ $\text{NH}_3(\text{aq})$ ; batch C d) 200 $\mu\text{l}$ Igepal $\text{NH}_4\text{OH}$ ; batch D (80 $\mu\text{l}$ TEOS and 1300 $\mu\text{l}$ Igepal CO-520 was used).....	65
<b>Figure 39</b> TEM images of iron oxide nanoparticles prepared using 1300 $\mu\text{l}$ Igepal CO-520, 80 $\mu\text{l}$ TEOS and two different amounts of $\text{NH}_3(\text{aq})$ a) 150 $\mu\text{l}$ $\text{NH}_3(\text{aq})$ ; batch C, b) and c) 200 $\mu\text{l}$ $\text{NH}_4\text{OH}$ ; batch D.....	66

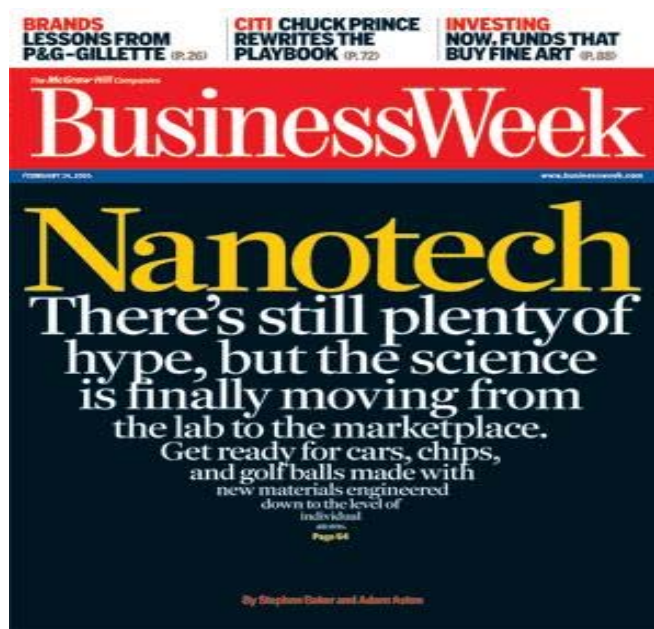
<b>Figure 40</b> The agglomerate size distribution of the silica coated iron oxide nanoparticles prepared using 1300 $\mu\text{l}$ Igepal CO-520, 80 $\mu\text{l}$ TEOS and 200 $\mu\text{l}$ of $\text{NH}_3(\text{aq})$ , batch D.....	67
<b>Figure 41</b> Photographs of $\text{SiO}_2$ coated $\text{Fe}_3\text{O}_4$ nanoparticle suspensions prepared using different amounts of $\text{NH}_3(\text{aq})$ a) 75 $\mu\text{l}$ $\text{NH}_3(\text{aq})$ ;vbatch A b) 100 $\mu\text{l}$ $\text{NH}_3(\text{aq})$ ; batch B c) 150 $\mu\text{l}$ $\text{NH}_3(\text{aq})$ ;batch C d) 200 $\mu\text{l}$ $\text{NH}_3(\text{aq})$ ; batch D.....	70

## CHAPTER 1

### INTRODUCTION

#### 1.1 Nanotechnology and Nanoparticles

On December 29, 1959, Professor Richard Feynman (1965 Nobel Prize winner in physics) presented a lecture entitled “There’s Plenty of Room at the Bottom” during the annual meeting of the American Physical Society at the California Institute of Technology (Caltech). He described a field that few researchers had thought much about, let alone investigated. Feynman presented the idea of manipulating and controlling things on an extremely small scale by building and shaping matter one atom at a time. [1]

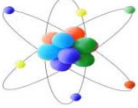

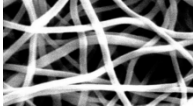
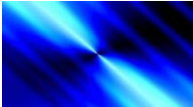
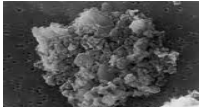


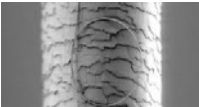


**Figure 1** This is a reference to what Feynman has said: “there is plenty of space at the bottom” and also to the failure of the “biotechnology age “in delivering what it promised.

Nanotechnology, [2] is facilitating technology which interested in nano-meter sized objects [3]. Nano is derived from the Greek word meaning “dwarf.” Nanotechnology is the research and development of materials, devices and systems that exhibit physical, chemical and biological properties[4]. In an effort to define the borders of this new and emerging discipline the National Nanotechnology Institute (NNI) proposed the limitation that truly “nanotechnology is the understanding and control of matter at dimensions of roughly 1 to 100 nm, where unique phenomena enable novel applications” [5].

Nanotechnology “the manipulation of matter on a near-atomic scale to produce new structures, materials, and devices” offers the promise of unprecedented scientific advancement for many sectors, such as medicine, consumer products, energy, materials, and manufacturing. Nanotechnology has the power not only to improve existing technologies, but to dramatically enhance the effectiveness of new applications [6].

Nanoparticles (NP) are collection of several atoms of a particular element in a given fashion [7]. Nanoparticles are defined as particles with size in the range of 1 to 100 nm at least in one of the three dimensions. Because of this very small size scale, they possess an immense surface area per unit volume, a high proportion of atoms in the surface and near surface layers, and the ability to exhibit quantum effects. The resulting unique properties of nanoparticles cannot be anticipated from a simple extrapolation of the properties of bulk materials. Nanoparticles exist with great chemical diversity in the form of metals, metal oxides, semiconductors, polymers, carbon materials, organics or biological. They also exhibit great morphological diversity with shapes such as spheres, cylinders, disks, platelets, hollow spheres and tubes, etc. [8]

<b>Table 1</b> Some Materials in Nanometers [4]	
<p>The Width of an Atom</p> 	1 nanometer (nm)
<p>The Width Across a DNA Molecule</p> 	2 nanometers
<p>The Width of a Wire in a Computer</p> 	100 nanometers
<p>The Wavelength of Ultraviolet Light</p> 	300 nanometers
<p>The Width of a Dust Particle</p> 	800 nanometers
<p>The Length of Some Bacteria</p> 	1,000 nanometers
<p>The Width of a Red Blood Cell</p> 	10,000 nanometers
<p>The Width of a Hair</p> 	75,000 to 100,000 nanometers

## 1.2 Magnetic Nanoparticles

Magnetic nanoparticles show many magnetic phenomena, a property that distinguishes them from their bulk counterparts and makes magnetic nanoparticles advantageous for usage in a variety of applications [9].

Magnetic nanoparticles research area include “magnetic fluids, catalysis, biotechnology/biomedicine, magnetic resonance imaging, data storage, and environmental remediation” [10].

Using particles of sizes smaller than 100 nm have some advantages because of their higher effective surface areas, high stability, improved tissular diffusion [11, 12]. Therefore, for *in vivo* biomedical applications, magnetic nanoparticles should be made of a non-immunogenic and non-toxic material to obtain biocompatibility. When particle sizes are too small, after injection particles remain in the circulation and they can also pass through the capillary systems of tissues and organs. By employing magnetic nanoparticles having a high magnetization, movement of the particles in the blood can be controlled with a magnetic field [13].

Directing the particles to a particular site in biological systems is a major problem of the use of nanoparticle therapy. A benefit of using magnetic nanoparticles is the use of localized magnetic field gradients. The magnetic nanoparticles are attracted to a chosen site, to hold them there until the therapy is complete and after that to remove them. [14].

In particular, magnetite nanoparticles have used for many important biomedical applications for example, drug delivery, magnetic resonance imaging (MRI) enhancement, cancer hyperthermia and magnetic separation [15, 16] due to their high chemical stability and non-toxicity property. In this respect, magnetite nanoparticles are essential to be stable in water, monodisperse, superparamagnetic and easy to produce in large scale [17].

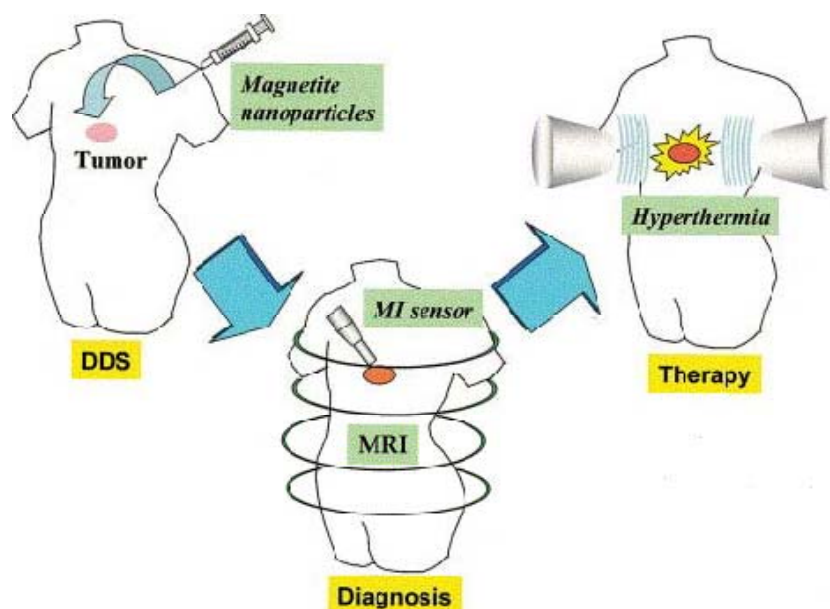
### 1.3 Applications of Magnetic Nanoparticles

Biological and medical (diagnostic and therapeutic) applications require the magnetic particles to be stable in water at neutral pH. The colloidal stability of this fluid will rely on two factors: first, the size of the particles must be very small so that precipitation which will occur because of the gravitation forces can be avoided. Second factor is the charge and surface chemistry. They give rise to both, steric and coulombic repulsions [18]. Additional constrictions to the magnetic nanoparticles used for biomedical applications depend on whether these particles will be used for *in vivo* or *in vitro* applications [12].

The nanoparticles must have some characteristics for biomedical applications, [19];

- They must be composed of “non-toxic” and “non-immunogenic” materials,
- Their size must be too small to allow them to remain in circulation after being injected into the body and also to pass through the capillary system to reach desired organs and tissues,
- They must have sufficient magnetization for their movement in the biological systems to be controlled by a magnetic field, thus they could be immobilized close to the affected tissue or area,
- The particles must exhibit superparamagnetic behavior at room temperature so that they prevent agglomeration within the body and they can also prevent blockage of blood vessels,
- They must be stable in water at neutral pH.

Schematic of magnetic nanoparticles applications is shown in Figure 2.



**Figure 2** Schematic of magnetic nanoparticles applications, (a) through the Drug Delivery Systems (DDS) functionalized MNP build up in the tumor tissue, (b) as a diagnosis tool for cancer by magnetic resonance imaging (MRI) or for magneto impedance (MI) sensor, (c) as a hyperthermia treatment for cancer [20].

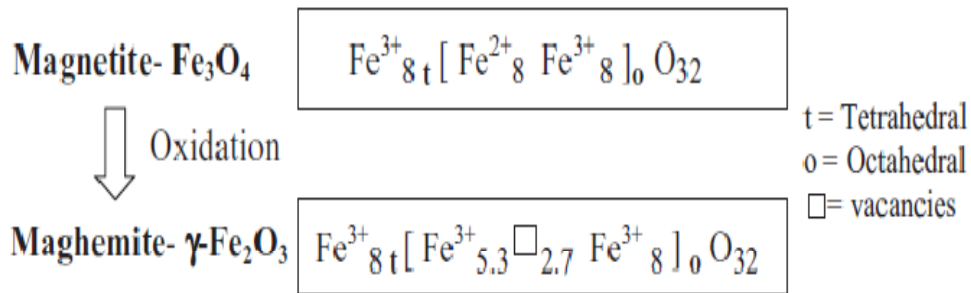
#### 1.4 Iron Oxide Magnetic Nanoparticles

Iron oxide magnetic nanoparticles produce attractive possibilities in biomedical applications. For example, cell labeling and separation, magnetic resonance imaging (MRI), targeted drug delivery and magnetic ferrofluids hyperthermia (MFH) [15, 21, 22]. Since they exhibit high saturation magnetization, low toxicity, and biocompatibility [23], magnetic iron oxide nanoparticles are promising materials to be used as magnetic targeted drug delivery carriers and



magnetic resonance imaging (MRI) contrast agents. Colloidal iron oxide nanoparticles have been investigated magnetic nanoparticles for biomedical applications because of their biocompatibility and their synthesis easy. These ferrite nanoparticles, typically composed of nanocrystalline magnetite ( $\text{Fe}_3\text{O}_4$ ) or maghemite ( $\gamma\text{Fe}_2\text{O}_3$ ) protected with a polymeric coating, have a “spinel crystal structure with oxygen ions forming a close-packed cubic lattice and iron ions located at interstices”. In the case of  $\text{Fe}_3\text{O}_4$ , electron hopping between the  $\text{Fe}^{2+}$  and  $\text{Fe}^{3+}$  ions that coexist at the octahedral sites yields magnetization. In addition to magnetic properties, the advantageously biocompatibility and biodegradability of these magnetic nanoparticles made huge contribution to their common use in biomedical applications. Utilization of free iron ions in the metabolism results in their addition to the body's iron stores and eventually incorporation by erythrocytes as hemoglobin, which allows safe use of these particles *in vivo* [22].

In the last decade, increased researches with several types of iron oxides have been executed in the field of magnetic nanoparticles (including the ferrimagnetic magnetite, ( $\text{Fe}^{\text{II}}\text{Fe}^{\text{III}}_2\text{O}_4$ ), which is superparamagnetic when the particle size is less than 15 nm),  $\alpha\text{-Fe}_2\text{O}_3$  (hematite, weakly ferromagnetic or antiferromagnetic),  $\gamma\text{-Fe}_2\text{O}_3$  (maghemite, ferrimagnetic),  $\text{FeO}$  (wüstite, antiferromagnetic),  $\varepsilon\text{-Fe}_2\text{O}_3$  and  $\beta\text{-Fe}_2\text{O}_3$ ) [24] which magnetite and maghemite is popular magnetic nanoparticles because their biocompatibility have been demonstrated [25]. Iron oxide particles such as magnetite ( $\text{Fe}_3\text{O}_4$ ) or its oxidized form maghemite ( $\gamma\text{-Fe}_2\text{O}_3$ ) are used for biomedical applications [12]. However, to control size, shape, stability, and dispersibility of nanoparticles is a “technological challenge” in required solvents. Magnetic iron oxide nanoparticles have a large surface-to-volume ratio so hold high surface energies. Therefore, they are disposed to aggregate for the purpose of minimize the surface energies. Furthermore, the naked iron oxide nanoparticles have high chemical activity, and they are also easily oxidized in air (especially magnetite), so that they lose of magnetism and dispersibility. For this reason, appropriate surface coating to protect the stability of magnetic iron oxide nanoparticles is very important [25].



**Figure 3** Chemical formula for the magnetite/maghemite system[12].

### 1.4.1 Maghemite

Maghemite ( $\gamma\text{-Fe}_2\text{O}_3$ ) has a cubic crystal structure similar to the inverse spinel crystal structure of magnetite and was the most common magnetic material used in magnetic recording media as of 1994, owing to the coercivity values of anisotropic maghemite nanoparticles (~200 to 400 Oe) [26]. Maghemite particles are usually prepared from  $\alpha\text{-Fe}_2\text{O}_3$  precursor particles first by partial reduction with  $\text{H}_2$  after that by oxidation in air at ~ 100 °C [27] or by spray pyrolysis methods [28] or by the ion exchange method [29].

### 1.4.2 Magnetite

Magnetite ( $\text{Fe}_3\text{O}_4$ ) is a black mineral which exhibits the strongest magnetism among the transition metal oxides[30]. Magnetite ( $\text{Fe}_3\text{O}_4$ ) is a mixed iron oxide ( $\text{FeO}\cdot\text{Fe}_2\text{O}_3$ ) with an inverse spinel crystal structure. In the inverse spinel structure, “half of the  $\text{Fe}^{+3}$  ions are tetrahedrally coordinated” and the other “half of the  $\text{Fe}^{+3}$  ions and all of the  $\text{Fe}^{+2}$  ions are octahedrally coordinated”. Each octahedral site has six nearest neighbor  $\text{O}^{-2}$  ions arranged on the corners of an octahedron, while each tetrahedral site has four nearest neighbor  $\text{O}^{-2}$  atoms

arranged on the corners of a tetrahedron [26]. The  $\text{Fe}_3\text{O}_4$  is ferrimagnetic at temperatures below 858 K [31].

Magnetite particles can be prepared by alkalizing stoichiometric mixtures of ferrous and ferric ions with aqueous  $\text{NH}_3$ , in aqueous solutions or in microemulsions at room temperature, by partial oxidation of aqueous ferrous hydroxide gel, or by some solid chemistry method  $\text{Fe}_3\text{O}_4$  (magnetite) [32].

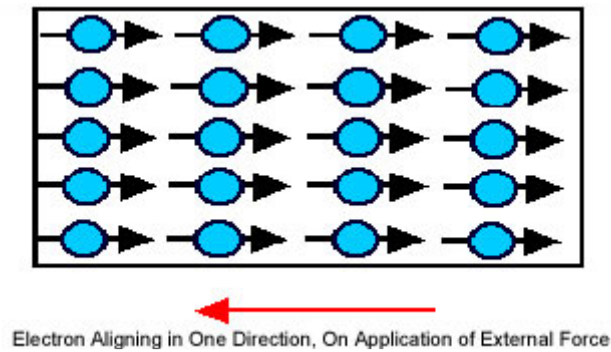
## **1.5 Magnetism and Magnetic Properties**

Magnetic nanoparticles have many typical magnetic properties. These are high magnetic susceptibility ( $\chi$ ), low Curie temperature, high coercivity, superparamagnetism, etc. [25, 33]

### **1.5.1 Diamagnetism**

The induction of a magnetic moment upon exposure to an external magnetic field defines diamagnetism [26]. Diamagnetism is very weak. However, it is a fundamental property of all matter. It is due to the non-cooperative behavior of orbiting electrons when exposed to an applied magnetic field. Diamagnetic materials have a negative magnetic susceptibility ( $\chi$ ), because of the direction of the induced magnetic moment upon exposure to a magnetic field [34]. When exposed to a field  $H$ , the orbiting electrons either accelerate or decelerate, so that their magnetic moments are in the opposite direction from the external field. Once the external field is removed, the diamagnetic material loses its magnetization, and a negative magnetization is produced, and because of this, the susceptibility

$\chi_m$  is  $< 0$  (order of  $-10^{-5}$ ) for a diamagnetic material, resulting in very low dipole moments [34-37].

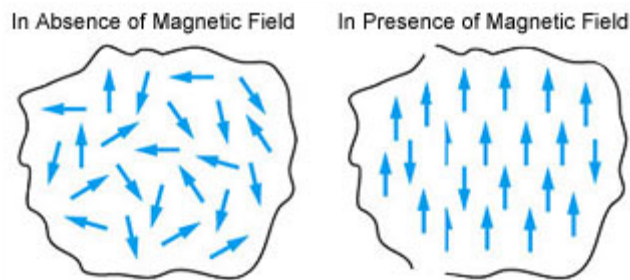


**Figure 4** Diamagnetism

### 1.5.2 Paramagnetism

Paramagnetism occurs in materials with permanent magnetic dipole moments, such as atoms or molecules with an odd number of electrons and atoms or ions with unfilled electron shells [38].

Some of the atoms or ions in the material have a net magnetic moment because of unpaired electrons in partially filled orbitals. However, the individual magnetic moments do not interact magnetically. When the field is removed, the net magnetization is zero. There is a partial alignment of the atomic magnetic moments in the direction of the field in the existence of a field, so a net positive magnetization and susceptibility  $\chi_m$  is  $> 0$  (order of  $10^{-5}$  to  $10^{-2}$ ) for paramagnetic materials [35].

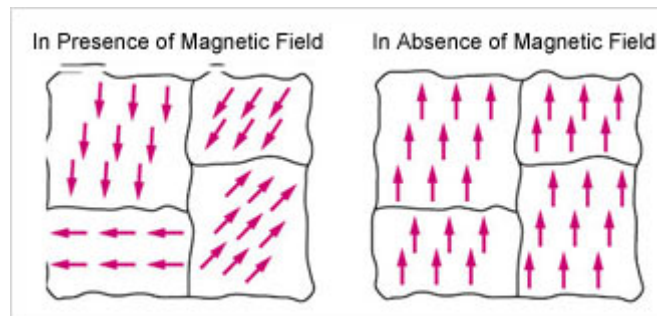


**Figure 5** Paramagnetism

### 1.5.3 Ferromagnetism and Ferrimagnetism

Both, ferromagnetic and ferrimagnetic materials contain unpaired electrons. Each domain is a single magnetic dipole which typically has dimensions of less than 100 nm [34].

Ferromagnetic materials exhibit parallel alignment of permanent magnetic property absence of the magnetic field. These moments originate from the overall contribution of electron spin and orbital magnetic moment [36]. Some of the typical ferromagnetic materials are Fe, Ni, and Co and many of their alloys. The best example of a ferromagnetic mineral is magnetite ( $\text{Fe}_3\text{O}_4$ ) [39]. In an equilibrated ferromagnetic or ferrimagnetic material the magnetic dipoles are organized in random directions; however, when a magnetic field is applied they are aligned even when the magnetic field is removed because the ambient thermal energy is insufficient to reorientate them (see Figure 6).



**Figure 6** Ferromagnetism

The magnetic dipole moments of a ferrimagnetic material are not totally canceling each other. Ferromagnetic materials have higher saturation magnetization values than ferrimagnetic materials [35].

#### 1.5.4 Antiferromagnetism

Antiferromagnetic materials are characterized by having a weak magnetic susceptibility of the order of paramagnetic materials. Examples of antiferromagnetic materials are transition metal compounds and some transition metal oxides ( $\text{CuCl}_2$ ,  $\text{CoO}$ ,  $\text{NiO}$ ). Antiferromagnetic materials are comprised of sublattices of atoms whose magnetic dipole moments are aligned antiparallel. This phenomenon of the “alignment of spin moments of neighboring atoms or ions in exactly opposite directions” is termed antiferromagnetism. The opposing magnetic moments cancel one another resulting in zero net magnetization of the material [36] and also the antiparallel arrangement of magnetic dipoles in antiferromagnetic materials is the cause for the small magnetic susceptibility of antiferromagnetic materials [40].

### 1.5.5 Superparamagnetism

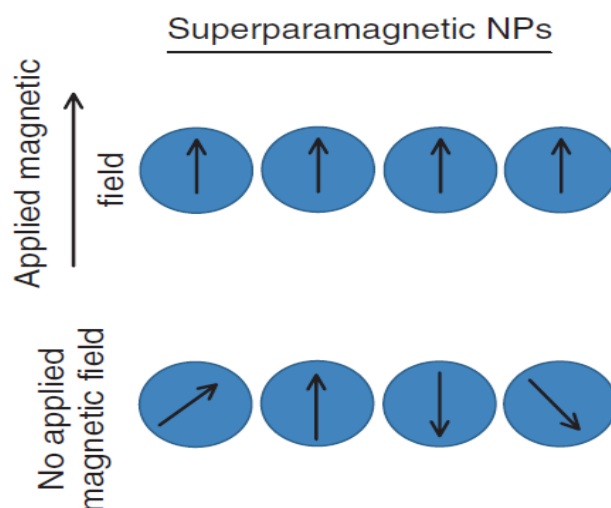
Superparamagnetic materials are a unique class of materials [26]. Superparamagnetism is a phenomenon by which “magnetic materials may behave similar to paramagnetism at temperatures below the Curie or the Neel temperature”. when the materials are comprised of very small crystallites (usually below 10 nm) superparamagnetism occurs at that, although the temperature is below the Curie or Neel temperatures, the thermal energy is enough to accomplish the coupling forces between neighboring atoms. It causes to change in the direction of magnetization of the all crystallite. The resulting fluctuations in the direction of magnetization lead to the magnetic field to average to zero. The material behaves in a similar to paramagnetism, but instead of each individual atom being independently influenced by an external magnetic field, the magnetic moment of the entire crystallite tends to align with the magnetic field. The crystalline anisotropy energy ( $KV$ ) is the energy which necessary to alter the direction of magnetization of a crystallite and depends both on the material properties and the crystallite size. When the crystallite size decreases, so that the crystalline anisotropy energy, material becomes superparamagnetic due to the decrease in the temperature [41]. The phenomenon of superparamagnetism is timescale-dependent due to the stochastic (random variable) nature of the thermal energy [39].

Superparamagnetic particles are uniformly magnetized along an easy axis and thermal energy causes the magnetization to switch between equivalent easy axes through an anisotropy barrier. This switching happens so quickly that the time average magnetic remanence is zero [42].

When the size of the nanoparticles is below a 10-20 nm, all of them becomes a single magnetic domain so, each particle shows superparamagnetic behavior and also their coercivity becomes zero because of their small size. These particles show same properties with the paramagnetic materials as mentioned but they have higher saturation magnetization values. Because of these features,

superparamagnetic nanoparticles find a broad range in the biomedical applications [10].

Generally, superparamagnetic particles (usually  $\gamma\text{-Fe}_2\text{O}_3$  and  $\text{Fe}_3\text{O}_4$ ) are used *in vivo* applications, because superparamagnetic material has no hysteresis loop like ferromagnetic materials. When the external magnetic field removed, its magnetization decreases to zero [43, 44].



**Figure 7** The magnetic moment of single-domain superparamagnetic nanoparticles aligns with the applied field. Superparamagnetic nanoparticles will exhibit no net magnetization due to rapid reversal of magnetic moment [45].



## 1.6 Synthesis of Iron Oxide Magnetic Nanoparticles

Magnetic properties of magnetic nanoparticles can be tailored by their particle sizes and size distributions. The particle sizes and size distributions of magnetic nanoparticles are in turn, affected by the synthesis route. For these reasons, various synthesis approaches have been improved producing magnetic iron oxide nanoparticles in order to obtain desired properties. Synthesis methods of magnetic iron oxide nanoparticles that have been improved include co-precipitation [25, 46], thermal decomposition [10], microemulsion route [46, 47], hydrothermal synthesis [25], polyols method [17], spray pyrolysis method [48] and continuous flow technique [23].

**Table 2** Comparison of the synthetic methods [10]

<b>Synthesis Methods</b>	<b>Co-precipitation</b>	<b>Thermal decomposition</b>	<b>Microemulsion</b>	<b>Hydrothermal</b>
<b>Reaction Temp. °C</b>	20-90	100-320	20-50	220
<b>Reaction Time</b>	Minutes	Hours-days	Hours	Hours-days
<b>Solvent</b>	Water	Organic solvents	Organic solvents	Water-ethanol
<b>Size distribution</b>	Relatively narrow	Very narrow	Relatively narrow	Very narrow
<b>Shape Control</b>	Not good	Very good	Good	Very good
<b>Yield</b>	High	High	Low	Medium

### 1.6.1 Thermal Decomposition Method

The decomposition of iron precursors in the presence of high boiling organic solvent has yielded significantly enhanced samples with good size control, narrow size distribution and good crystallinity of individual and dispersible magnetic iron oxide nanoparticles. Magnetic nanoparticles produced by thermal decomposition method could be potentially used for biomedical applications like magnetic resonance imaging or magnetic cell separation [12].

Monodisperse magnetic nanocrystals with smaller size can be synthesized by thermal decomposition of organometallic compounds in high-boiling organic solvents and stabilizing surfactants [49-51]. The organometallic precursors include “metal acetylacetonates,  $[M(\text{acac})_n]$ , ( $M=\text{Fe, Mn, Co, Ni, Cr}$ ;  $n=2$  or  $3$ ,  $\text{acac}=\text{acetylacetonate}$ ), metal cupferronates  $[M_x\text{Cup}_x]$  ( $M=\text{metal ion}$ ;  $\text{Cup}=\text{N-nitrosophenylhydroxylamine}$ ,  $\text{C}_6\text{H}_5\text{N}(\text{NO})\text{O}^-$ ) [52], or carbonyls” [53]. Thermal decomposition of iron pentacarbonyl  $[\text{Fe}(\text{CO})_5]$  has been used for the preparation of monodisperse  $\gamma\text{-Fe}_2\text{O}_3$  nanoparticles with average diameters ranging from 4 to 16 nm by control of the molar ratio of metal precursor to surfactant,  $[\text{Fe}(\text{CO})_5]$  and oleic acid respectively [54]. Since  $\text{Fe}(\text{CO})_5$  is very expensive and toxic, some attempts have been made to replace  $\text{Fe}(\text{CO})_5$  with iron acetylacetonate  $[\text{Fe}(\text{acac})_3]$  [55]. The most often used surfactants are fatty acids [56], oleic acid [57], and hexadecylamine [58]. In principle, the control of the size and morphology of magnetic nanoparticles can be reached by selecting the favorable decisive parameters, namely, the ratios of the starting reagents including organometallic compounds, surfactant, and solvent. The reaction temperature, reaction time and aging period may also be considerable for the certain control of size and morphology [10].

Thermal decomposition seems the best method developed to date for size and morphology control of nanoparticles. Also, the yield of production is high. The production of organic soluble nanoparticles is one of the major disadvantages of this method. Uses of them in biological fields besides surface treatment is needed

after synthesis. Moreover, thermal decomposition methods usually cause to complicated processes or require considerably high temperatures [46].

## **1.7 Surface Modification of Iron Oxide Magnetic Nanoparticles**

Small particles tend to form agglomerates to reduce the energy related with the high surface area to volume ratio of the nanosized particles. Additionally, metallic nanoparticles have high chemical activity, and they are prone to oxidation in air, leading loss of dispersibility and magnetism. Thus, it is crucial for many applications to develop protection strategies for chemical stabilization of the naked magnetic nanoparticles against degradation during or after the synthesis. These strategies involve coating or grafting of with organic molecules [25], including “small organic molecules or surfactants” [25], polymers [59], and “biomolecules or coating with an inorganic layer” [25], such as silica, metal [60] or nonmetal elementary substance, metal oxide or metal sulfide. Aplicatively, it is significant in many cases the protecting shells stabilize the magnetic iron oxide nanoparticles, and they can be used for functionalization [10, 25] An inert silica coating on the surface of magnetite nanoparticles avoid their aggregation in liquid and enhance the chemical stability. At the same time, the silanol surfaces can be changed with different coupling agents to covalently bond specific bioligands to the surfaces of the magnetic nanoparticles [61, 62]

### **1.7.1.1 Silica Coating**

Chemical stability, low coercivity, strong magnetization, and biocompatibility of the dispersed magnetic nanoparticles are necessary for all biomedical application of magnetic colloids. In principal, silica coated magnetite or maghemite nanoparticles, comply with these requirements [63].

Coating magnetic nanoparticles with silica is becoming a promising and important approach in the development of magnetic nanoparticles for both fundamental study and technology application.

Firstly, silica formed on the surface of magnetic nanoparticles could screen the magnetic dipolar attraction between magnetic nanoparticles, which favors the dispersion of magnetic nanoparticles in liquid media and protects them from leaching in an acidic environment.

Secondly, due to the existence of abundant silanol groups on the silica layer, silica-coated magnetic nanoparticles could be easily activated to provide the surface of silica-coated magnetic nanoparticles with various functional groups.

Finally, the most important property of silica layer is provide a chemically inert surface for magnetic nanoparticles in biological systems [64].

In general, to prepare of silica-coated magnetic nanoparticles, there are four main methods [64].

***The first method*** is a sol–gel method, in literature, this method is also named as Stöber method. In sol-gel method, the silicon alkoxides used as the source of silica matrix [65].

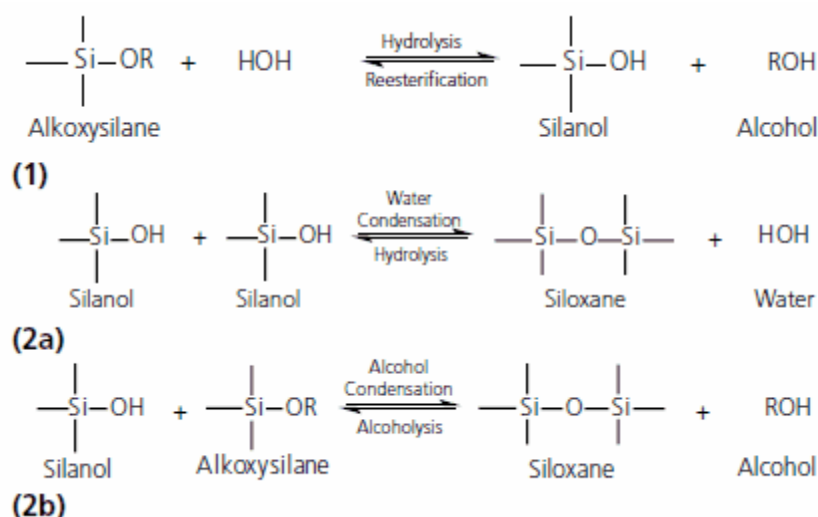
***The second method*** is based on either in situ formation of magnetic nanoparticles inside the pores of pre-synthesized silica using metal compounds (i.e. salts, complex or alkoxides) as the source of magnetic phase under certain conditions [66].

***The third method*** is an aerosol pyrolysis method. In this method, silica coated magnetic nanoparticles were prepared by aerosol pyrolysis of a precursor mixture composed of silicon alkoxides and metal compound in a flame environment [67].

More recently, *the fourth method* is microemulsion method. In this method, micelles or inverse micelles are used like a mini-reactor. They prepare the silica coated magnetic nanoparticles [68-70].

### 1.8 Sol-Gel Process

The sol- gel process is a term which consists of dispersion of solid nanoparticles in a liquid 'sol' and agglomeration of these nanoparticles together in order to provide the formation of continuous three-dimensional network prolonging in the liquid phase 'gel'. In sol gel process, the series of hydrolysis and condensation reactions of an alkoxide proceed according to the reaction scheme shown in Figure 8. Here, alkoxy silanes are used as an example but all of the metal alkoxides react similarly [71]. Alkoxy silanes such as tetramethoxysilane (TMOS) and tetraethoxysilane (TEOS) are the most widely used metal alkoxides. With the addition of water to the silane solution under acidic, neutral and basic conditions, hydrolysis step of the process is started.



**Figure 8** Sol gel general reaction mechanism

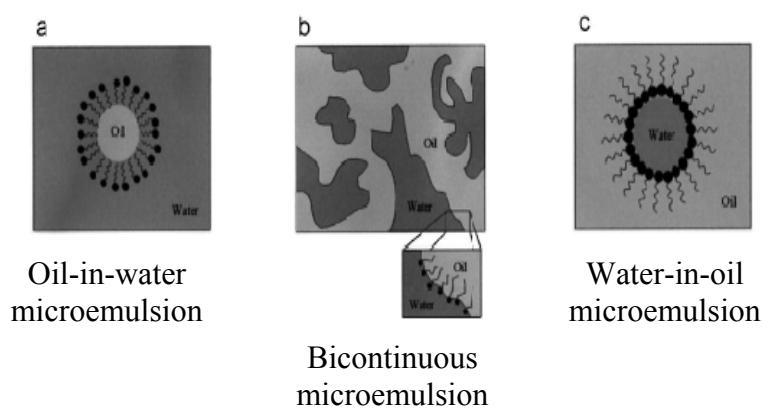
Catalyst is not needed for the hydrolysis and condensation reactions of most metal alkoxides because of their fast rates of reaction. On the other hand, either an acidic or a basic catalyst is needed for the hydrolysis of alkoxysilanes due to their slow rates of reaction. Despite the fact that sol-gel reactions do not require special conditions, that is, they can be done in a beaker, these reactions can be affected by the amount of acid catalyst, the amount of water, the addition of network modifier, and changing the effects of solvent used. Room temperature is enough for reactions to happen and only mild temperatures are required to solidify the gel to remove water-alcohol content occurred during the reaction process. In order to modify quality of the materials prepared by sol gel methods easily, an organically recovered alkoxide or a changeable arm metalloid (for example, an alkoxyborate instead of an alkoxysilane).

## **1.9 Microemulsion**

Microemulsions are thermodynamically stable isotropic dispersion of two immiscible water and oil phases with the surfactant molecules generating a monolayer at the interface between the oil and water by the dissolution of hydrophobic head groups in the oil phase and hydrophilic head groups in the aqueous phase. Several types of self-assembled structures ranging from (inverted) spherical and cylindrical micelles to lamellar phases and bicontinuous microemulsions, which exist together with mainly oil or aqueous phases, may be formed in the water/surfactant or oil/surfactant binary systems. [72]. Due to the formation of a transparent solution between water and oil, the surfactant molecule reduces the interfacial tension between these phases. The water nanodroplets contain reagents having a function of nanoreactor and these reagents result in the formation of rapid coalescence which allows the mixing, the precipitation reaction and the aggregation processes during the synthesis of magnetic nanoparticles. The spherical shape of the water pool is formed and the wall of nanodroplets are enclosed by the surfactant molecules. During the collision and

aggregation process, these nanodroplet walls by acting as cages prevent the growing of the particles and thus they assist with the reduction of average size of the nanoparticles. By this, changing the size of water pool provides the control of size of the spherical nanoparticles.

[46].



**Figure 9** a) oil-in-water microemulsion, b) bicontinuous microemulsion, and c) water-in-oil microemulsion [5].

Figure 9 shows of the three types of microemulsions. In each structure, interfacial surfactant monolayer separates the oil and water droplets. When the volume fraction of oil is low, oil in water microemulsion droplets are seen, on the other hand, when the volume fraction of water is low, water in oil microemulsion droplets are seen. In systems when amount of water and oil are similar, a bicontinuous microemulsion may result.

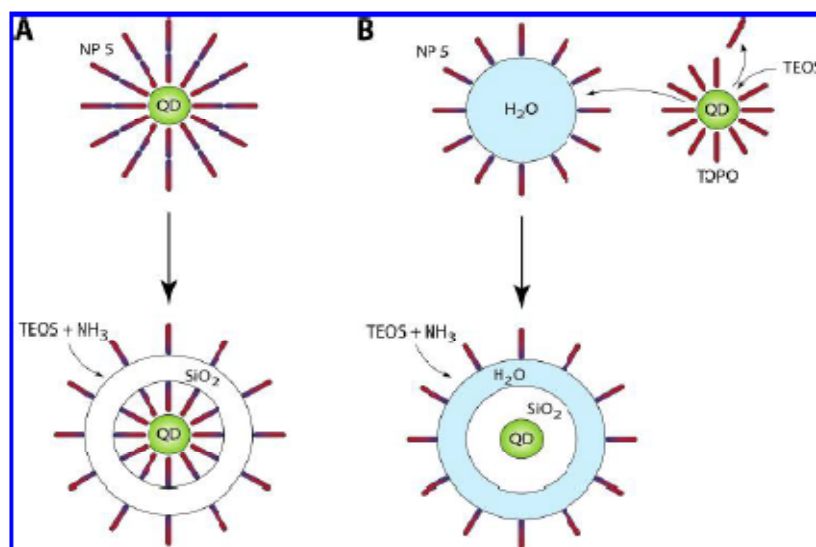
### 1.9.1 Silica Coating Through Inverse Microemulsion

Synthesis of monodispersed silica-coated nanoparticles has been achieved by water-in-oil microemulsion (w/o), or inverse microemulsion [68, 69, 73]. Inverse microemulsion method is best method for coating magnetic nanoparticles with thin layer [74]. This method involves the use of non-ionic surfactants for the formation of inverse microemulsion for the preparation of magnetic nanoparticles or their suspensions, where silica coating around the magnetic nanoparticles is produced by hydrolysis and condensation of tetraethyl orthosilicate (TEOS).

This method is also becoming increasingly preferred for the synthesis of core-shell complex structures and has recently been used for the synthesis of core-shell iron oxide-silica nanoparticles [73, 75-77]. For example, M. Zhang and his co-workers synthesized “ultra thin silica coated magnetic nanoparticles with a ~ 2 nm thin silica shell”. They transferred iron oxide nanoparticles to cyclohexane, containing an excess amount of surfactant (Igepal CO-520) and added ammonium hydroxide was introduced to form reverse microemulsion solution. TEOS was then added and stirred for 48 h. Silica shells slowly developed around the cores [77].

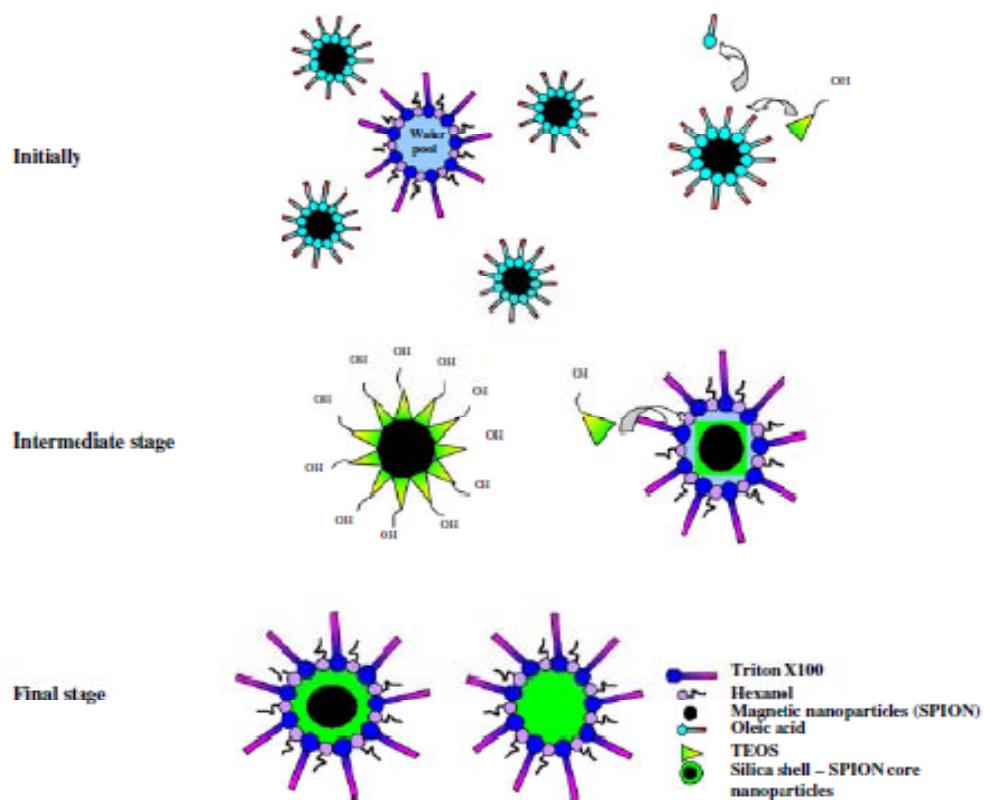
Most of the researchers suggest two hypothetical mechanisms for the formation of core-silica shell nanoparticles by inverse microemulsion. First one includes phase transfer without ligand exchange and second one, the phase transfer with ligand exchange. For the first mechanism, Darbandi and his co-workers have suggested that an inverse bilayer of the surfactants (NP-5) are formed around the hydrophobic ligands of the quantum dots. When ammonia and TEOS are added silica growth occurs between the layers (Figure 10-a). Selvan et al. suggested the same mechanism for quantum dots.





**Figure 10** Scheme of the two possible mechanism for silica growth on quantum dots [76].

For the second mechanism, Darbandi et al. suggested that the inverse microemulsion is formed initially and on addition of TEOS, hydrophobic ligands on the surface on the quantum dots are exchanged by TEOS. Then, quantum dots solubilized in oil phase are transferred to the water phase of the microemulsion (Figure 10-b). Toprak et al. also has applied the same mechanism for the iron oxide nanoparticles (Figure 11) [75, 76, 78].



**Figure 11** Scheme of the mechanism for the formation of iron oxide core-silica shell nanoparticles [78].

### **1.9.2 Aim of the Study**

In this study, the synthesis of silica coated particles, having overall size less than 50 nm, highly monodisperse, and non-aggregated single core-shell nanoparticles was our aim. For that reason, first small sized and mono dispersed iron oxide magnetic nanoparticles were synthesized by thermal decomposition and subsequently these synthesized iron oxide nanoparticles were coated with ultra thin silica by reverse microemulsion method. To obtain monodispersed and well defined nanoparticles, different silica coating experimental conditions were tried and the influence of the amount of Igepal CO-520, aqueous  $\text{NH}_3$  and TEOS was examined. The magnetic nanoparticles were characterized by transmission electron microscopic method (TEM).

## CHAPTER 2

### EXPERIMENTAL

#### 2.1 Chemicals and Reagents

All the chemicals and reagents used in this study were of analytical grade. 18 M $\Omega$ ·cm de-ionized water obtained from a Millipore water purification system was used during the synthesis and silica coating of magnetite nanoparticles. 10% HNO<sub>3</sub> and distilled water was preferred for cleaning of all the glassware and plastic ware which were kept at least 24 h in the 10% HNO<sub>3</sub> and then rinsing five times with distilled water.

##### 2.1.1 Synthesis of Iron Oxide Nanoparticles

The following chemicals and materials were used for the sythnesis of iron oxide nanoparticles by Thermal Decomposition Method 1

- i. **Ferric acetylacetonate, Tris(acetylacetonato)Iron (III), Fe(acac)<sub>3</sub>**, 97%, Fluka
- ii. **1,2 Hexadecanediol, technical grade 90%**, Sigma-Aldrich
- iii. **Oleic acid, (9Z)-Octadec-9-enoic acid**, analytical standard, Fluka
- iv. **Oleylamine, (Z)-9-Octadecen-1-amine**, technical grade, 70%, Fluka
- v. **Diphenylether**, 99%, Sigma-Aldrich
- vi. **Hexane (C<sub>6</sub>H<sub>14</sub>)**, Riedel- de Haen
- vii. **Ethanol (C<sub>2</sub>H<sub>5</sub>OH)**, 99.5%, Sigma-Aldrich

- viii. **Toluene (C<sub>6</sub>H<sub>5</sub>CH<sub>3</sub>), 99.0%, Merck**
- ix. **N<sub>2</sub> gas, Linde Gas Company.**

The following chemicals and materials were used for the sythesis of iron oxide nanoparticles by Thermal Decomposition Method 2

- i. **Ferric acetylacetonate, Tris(acetylacetonato)Iron (III), Fe(acac)<sub>3</sub>, 97%, Fluka**
- ii. **Oleylamine, (Z)-9-Octadecen-1-amine, technical grade, 70%, Fluka.**
- iii. **Benzylether, (C<sub>6</sub>H<sub>5</sub>CH<sub>2</sub>)<sub>2</sub>O, 99%, Sigma-Aldrich.**
- iv. **Ethanol (C<sub>2</sub>H<sub>5</sub>OH), 99.5%, Sigma-Aldrich.**
- v. **Hexane (C<sub>6</sub>H<sub>14</sub>), Riedel- de Haen.**
- vi. **Toluene (C<sub>6</sub>H<sub>5</sub>CH<sub>3</sub>), 99.0%, Merck**
- vii. **N<sub>2</sub> gas, Linde Gas Company.**

The following chemicals and materials were used for the Silica Coating on Iron Oxide Nanoparticles by Reverse Microemulsion Method

- i. **Tetraethyl ortosilicate, TEOS, Si(OC<sub>2</sub>H<sub>5</sub>)<sub>4</sub>, 98%, Aldrich**
- ii. **Ethanol (C<sub>2</sub>H<sub>5</sub>OH), 99.5%, Sigma-Aldrich**
- iii. **Cyclohexane, 99 %, Sigma-Aldrich**
- iv. **Ammonia Solution, 25% extra pure, Merck**
- v. **Acetone, 99%, Sigma-Aldrich**
- vi. **1-Butanol, 99%, Sigma-Aldrich**
- vii. **1-Propanol, 99 %, Merck**
- viii. **Igepal CO-520, Sigma- Aldrich**

## 2.2 Instrumentation

### 2.2.1 Centrifuge

Sigma 2-16 model centrifuge with maximum 13500 rpm rotating speed was used to separate precipitated nanoparticles.

### 2.2.2 Transmission Electron Microscope (TEM)

JEOL 2100 F Transmission Emission Microscopy (TEM) was operated at 200 kV, at METU Central Laboratory was used for shape and size characterization of nanoparticles. 200 mesh holey carbon coated grid and 200 mesh lacey carbon coated grid were used for analysis. Samples were dried on grid at room temperature for 24 hours before performing TEM analysis.

Number-length (arithmetic) mean size ( $D[1,0]$ ) of iron oxide and silica coated iron oxide nanoparticles were determined from the TEM images using the following formula 2.2.1.1.

$$D[1,0]= \frac{\sum d_i N_i}{\sum N_i} \dots\dots\dots(2.2.2.1)$$

$d_i$  is the diameter of a nanoparticle and  $N_i$  is the number of nanoparticles. In order to explain the calculations, imagine three spheres of diameters 1, 2 and 3 units. The average size of these three spheres are 2.00. It is calculated by summing all the diameters ( $\sum d = 1 + 2 + 3$ ) and dividing by the number of particles ( $n=3$ ). This is a number mean (number – length mean). The number-length mean size is also known as the arithmetic mean [79].

### **2.2.3 X-Ray Photoelectron Spectroscopy (XPS)**

PHI 5000 Versa Probe, surface analyzer instrument provides information about surface layer of iron oxide and silica coated iron oxide nanoparticles at METU Central Laboratory.

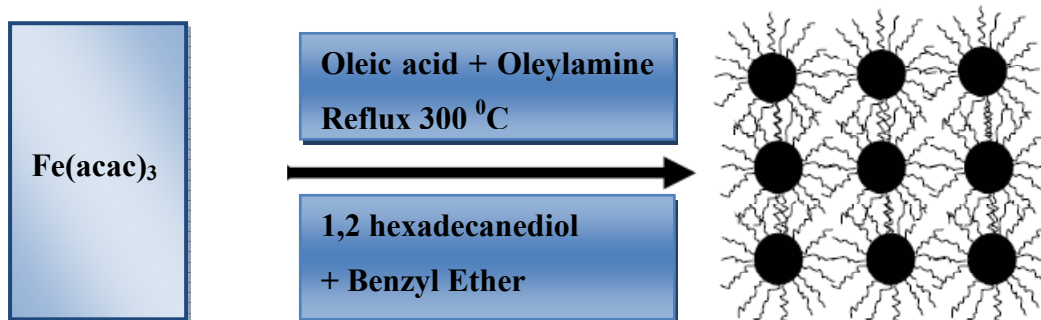
### **2.2.4 Particle Size Analyzer (Zeta Sizer)**

Malvern Zeta Sizer Nano ZS90 was used for the determination of the particle size of iron oxide and silica coated iron oxide nanoparticles at METU Central Laboratory.

## **2.3 Procedure**

### **2.3.1 Synthesis of Iron Oxide Nanoparticles by Thermal Decomposition Method 1**

353.17 mg of  $\text{Fe}(\text{acac})_3$ , 1.2922 g of 1,2-hexadecanediol, 847.39 mg of oleic acid (b.p= 360°C), 802.47 mg oleylamine and 10 mL of benzyl ether were mixed in a three necked flask.  $\text{Fe}(\text{acac})_3$  was used as an iron precursor, 1,2 hexadecanediol and oleylamine were used as reducing agents, oleic acid was used as a surfactant and benzyl ether was used as an organic solvent. The flask was heated to 200°C and held at that temperature for 30 minutes under mechanical stirring and a flow of  $\text{N}_2$  gas. After the 30 minutes holding, the mixture was maintained under the flow of  $\text{N}_2$  gas and the solution was heated to 298°C. The flask was maintained at the refluxing temperature of 298°C for 30 min. At the end, the solution was cooled down to room temperature. Particles were washed with ethanol and centrifuged for 10 min at 7000 rpm. Obtained nanoparticles were dispersed in hexane [80].



**Figure 12** Scheme for synthesis of  $\text{Fe}_3\text{O}_4$  nanoparticles



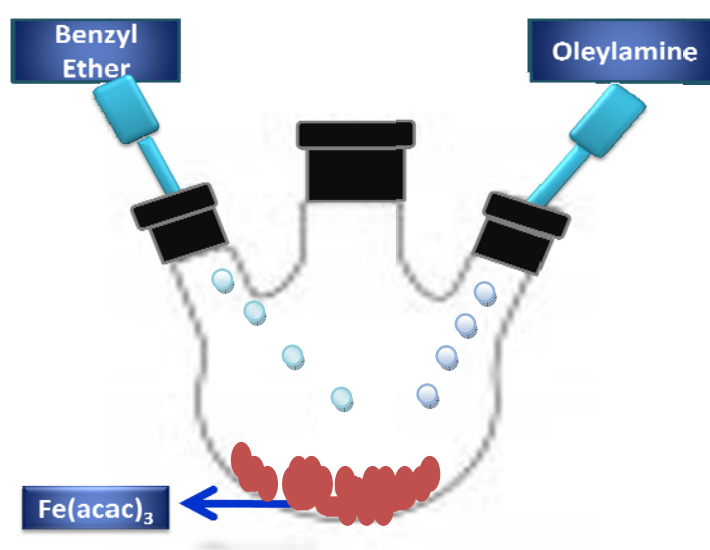
**Figure 13** Experimental setup for the synthesis of magnetic iron oxide nanoparticles with Thermal Decomposition Method



### 2.3.2 Synthesis of Iron Oxide Nanoparticles by Thermal Decomposition Method 2

In a typical synthesis of magnetic iron oxide NPs,  $\text{Fe}(\text{acac})_3$  (1 mmol) was dissolved in 5 mL of benzyl ether and 5 mL of oleylamine (Figure 14). 7 broken glass pieces, approximately  $50 \text{ mm}^2$ , were used. These boiling stones are renewed for each new synthesis, because of the adsorption of the nanoparticles on the glass surface.

The solution was dehydrated at  $110 \text{ }^\circ\text{C}$  for 1 h under  $\text{N}_2$  atmosphere.  $\text{N}_2$  gas flow rate was adjusted to 100 ml/min. Then heated quickly to  $300 \text{ }^\circ\text{C}$  at a heating rate of  $20 \text{ }^\circ\text{C}/\text{min}$ , aged at this temperature for 1 h and the solution color became black, suggesting that the magnetic iron oxide (most likely magnetite) nanoparticles were being formed. After refluxing for 1 h, the solution was allowed to cool down to room temperature. The iron oxide NPs were extracted upon the addition of ethanol, followed by centrifuging. The iron oxide NPs were dispersed in nonpolar solvent hexane. Finally, the product was dispersed in cyclohexane [81].



**Figure 14** The synthesis of magnetite nanoparticles

### 2.3.3 Silica Coating on Iron Oxide Nanoparticles by Reverse Microemulsion Method

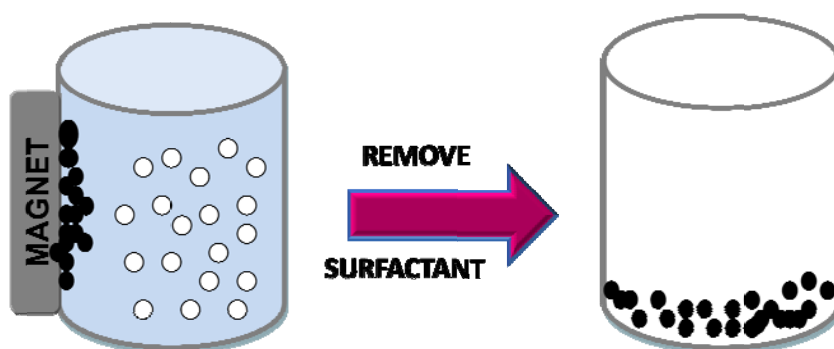
After synthesizing magnetic iron oxide nanoparticles, they were coated with silica. Firstly, 1500  $\mu\text{l}$  of Igepal CO-520 was dispersed in 10 ml cyclohexane by sonication for 15 minutes. Secondly, 467  $\mu\text{l}$  of iron oxide stock solution in cyclohexane, and 100  $\mu\text{l}$  of TEOS were added in a beaker and a brown transparent solution was formed. The mixture solution was stirred under 600 rpm for thirty minutes and after that the microemulsion system was formed. Thirdly, 150  $\mu\text{l}$  of aqueous  $\text{NH}_3$  (%25) was added dropwise while stirring vigorously.

The silica growth was completed after 24 h of stirring at room temperature.



**Figure 15** Microemulsion system was formed.

The resulting silica coated iron oxide nanoparticles isolated from the microemulsion using acetone, and they were collected using magnetic separation (Figure 16) and resultant precipitate of silica coated iron oxide composite particles was washed in sequence with 1-butanol, 1-propanol, ethanol and water and subject to centrifugation at 6000 rpm for 10 minutes to remove any surfactant and unreacted molecules [76]. For the washing procedure, the ultrasonic treatment was a necessary step because it enabled to disperse the precipitate in the solvent and it also helped to remove the adsorbed molecules from the surface of final product [82].



**Figure 16** Magnetic separation; a magnet is attached to the container wall of a solution of  $\text{SiO}_2\text{-Fe}_3\text{O}_4$  nanoparticles (•) and acetone (◦).

## CHAPTER 3

### RESULTS AND DISCUSSION

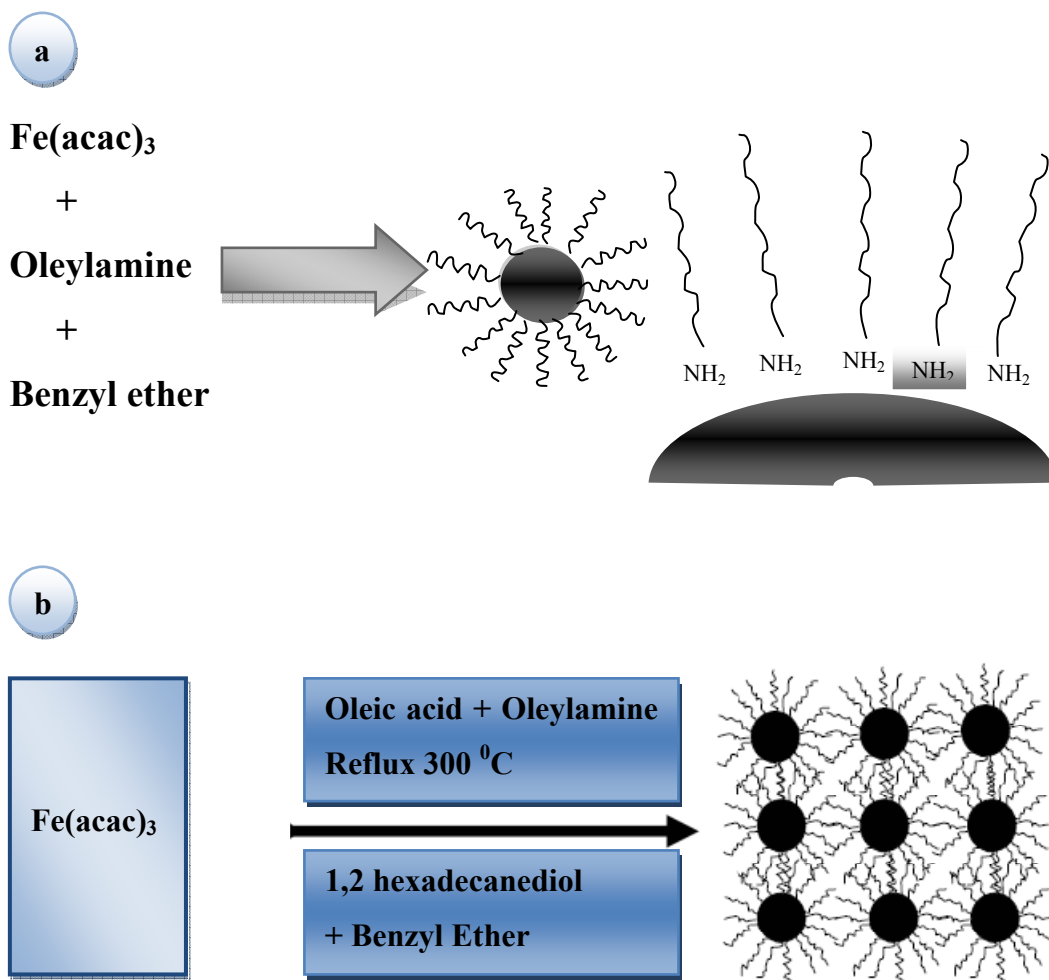
In this study, firstly magnetic iron oxide nanoparticles were synthesized by thermal decomposition method. Synthesized nanoparticles were then coated with silica through reverse microemulsion method and different reaction conditions for the microemulsion synthesis were studied and the effect of reaction conditions on the size of the silica coated iron oxide nanoparticles agglomerates were investigated.

#### **3.1 Synthesis of Iron Oxide Nanoparticles by Thermal Decomposition Method**

Thermal Decomposition method was used for the synthesis of monodispersed and small sized iron oxide nanoparticles in which chemical reduction of iron (III) acetylacetonate ( $\text{Fe}(\text{acac})_3$ ) takes place at high temperature in solution phase in the presence of oleic acid and oleylamine as surfactants. The particle size of nanoparticles can be controlled by systematically adjusting the reaction parameters, such as time, temperature and the types of reagents and stabilizing surfactants. At the beginning of the experiments the formation of a dark colored suspension in hexane was the criteria of success. Afterwards the thorough characterization was done by TEM measurements. Thermal decomposition method was used previously in our group (Method 1). In this thesis an economic preparation of the monodisperse iron oxide nanoparticles without using external expensive reducing reagent was tried (Method 2).

It is known from literature that for biomedical applications, magnetite would be preferred over maghemite because of its higher saturation magnetization and susceptibility [83]. Therefore, although both maghemite and magnetite could be prepared successfully using thermal decomposition method, we focused on the synthesis and characterization of magnetite as these particles were aimed to be used in biomedical applications. Hence, N<sub>2</sub> gas was purged through reaction medium during the synthesis in order to prevent oxidation of magnetite to maghemite.

For reduction two approaches were tried. In Method 1, 1,2-hexadecanediol was used together with oleylamine whereas only oleylamine was used in Method 2. Since 1,2-hexadecanediol is an expensive chemical, we tried to eliminate its usage in Method 2. In thermal decomposition, high temperature conditions are required. So, benzyl ether (Boiling points of benzyl ether is 298 °C) was used. During synthesis, the solvent was heated until boiling and tried to be kept at that temperature. The sizes of the particles were expected to grow with increasing reaction temperature due to the increase in the rate of reaction. Nanoparticle formation is shown schematically in Figure 17.

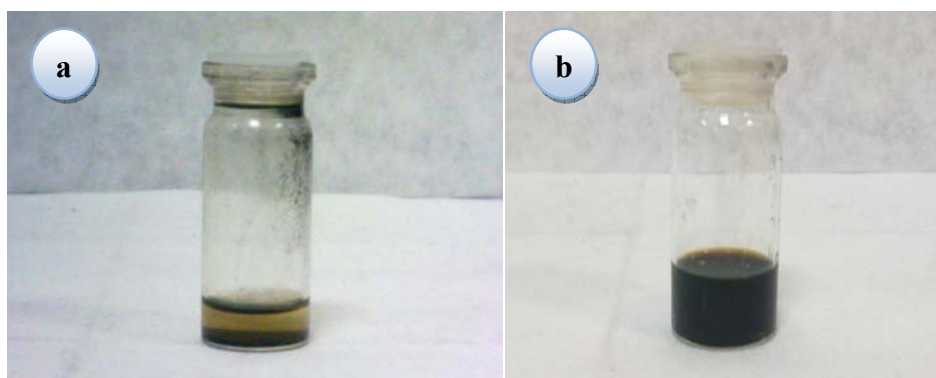


**Figure 17** Synthesis of iron oxide nanoparticles a) Method 2, b) Method 1

The first important factor in the synthesis was the rate of heating to reach the decomposition temperature to accomplish fast nucleation and growth of the nuclei which is the key factor for obtaining small and homogeneous nanoparticles. If the solutions were heated directly to reflux from room temperature, the nucleation of iron oxide particles and growth of nuclei under these reaction circumstances would not be fast enough and wide size distribution could be obtained [52, 91].

Therefore to make monodisperse nanoparticles, the mixtures were first heated to low temperatures as 200 °C (Method 1) and 110 °C (Method 2) and kept at that temperature for one hour before they were heated to reflux at 300 °C .

The second critical factor for the synthesis was to bring the system to 300 °C and maintain it there for at least one hour. Thus, the usage of the correct distillation column was significant to reach the temperature of 300 °C. Two distillation columns having the length of approximately 15 cm and 25 cm were tried. When distillation column with a length of 15 cm was used, most of the solvent was evaporated and reaction were ended after a short period of time without reaching 300 °C. When a length of about 25 cm distillation column was used refluxing process was achieved properly and the reaction was completed after a controlled heating period. In both cases the nanoparticles synthesized in the reactor were washed and placed into the hexane. Their appearances are given in Figure 18-a and Figure 18-b.



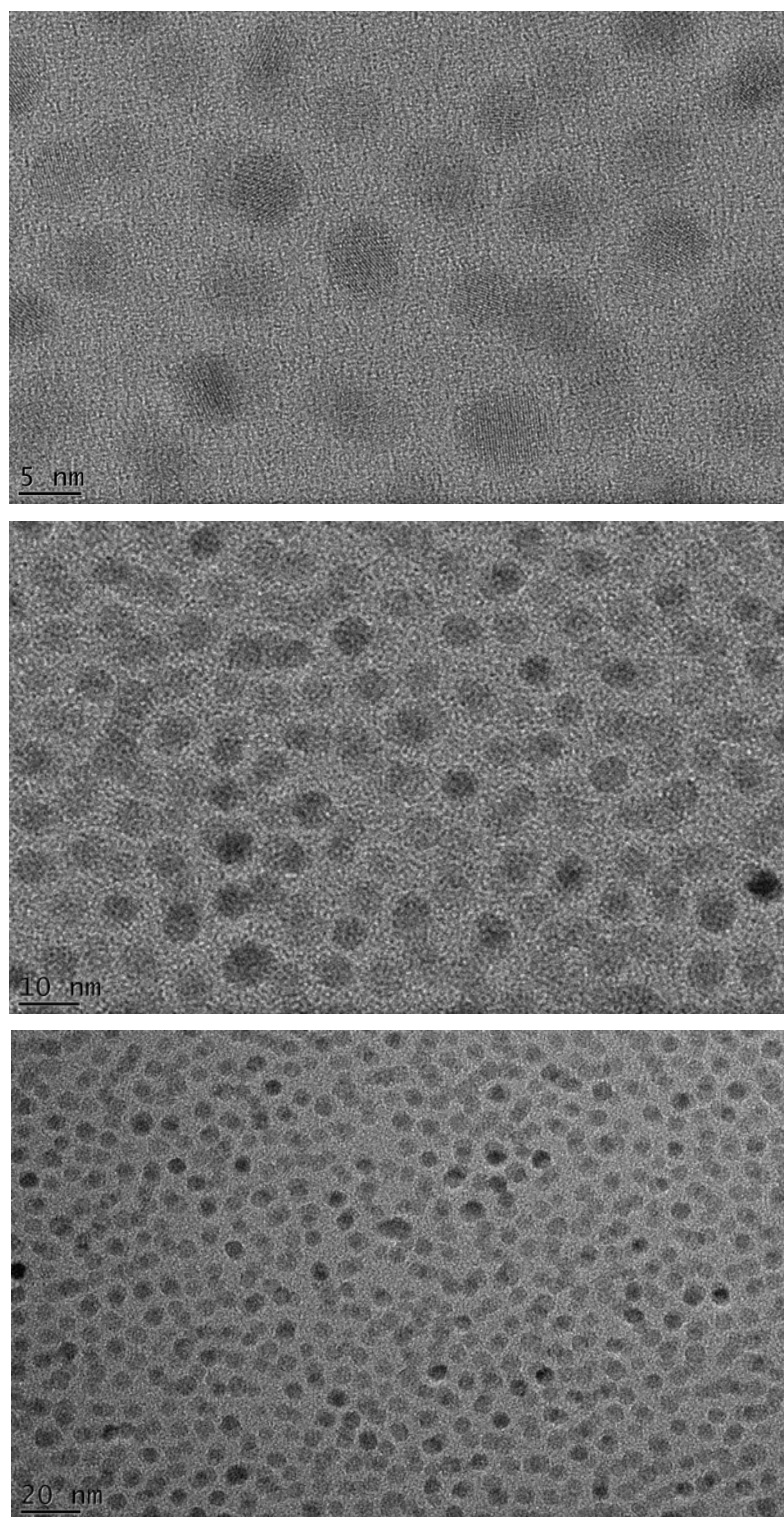
**Figure 18** Picture of a) heavily agglomerated iron oxide particles using 15 cm-column b) Stable suspension of the iron oxide nanoparticles using 25 cm-column

When a length of 25 cm distillation column was used, the size and shape of the iron oxide nanoparticles were controlled effectively and they were dispersed in

the hexane properly as shown in Figure 18-b. On the other hand with a shorter distillation column the particles were heavily agglomerated in hexane, Figure 18-a. Besides, we were used as boiling stones, providing nucleation sites therefore the mixture solution boils smoothly without bumping and it prevent loss of the solution.

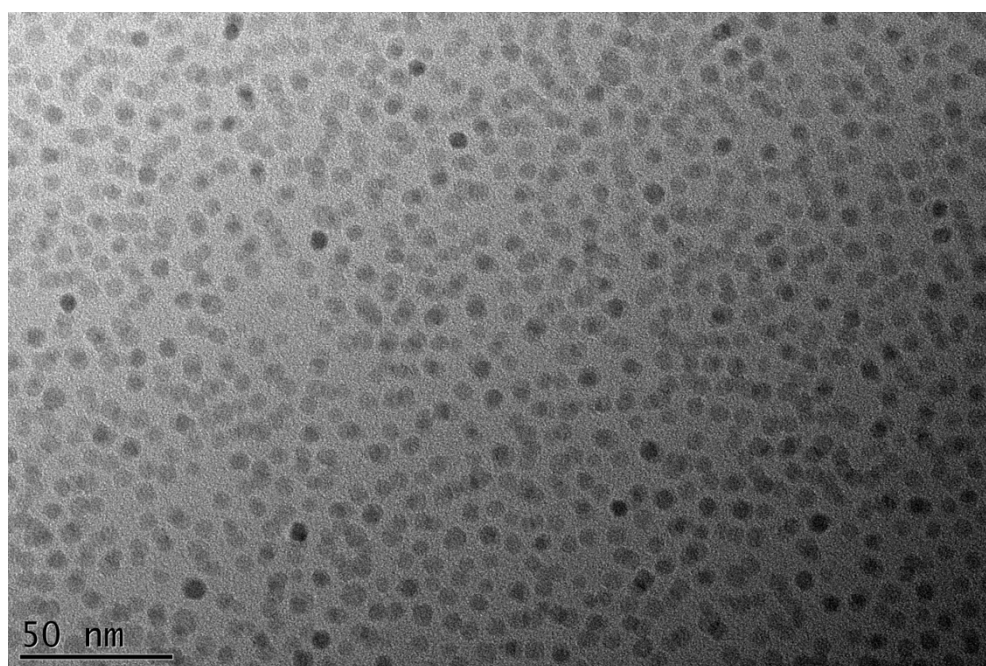
Transmission Electron Microscopy was used for the characterization of particle size and shape of the particles. TEM images of the particles prepared with Method 2 at three different magnification level are shown in Figure 19-a,b,c.





**Figure 19** TEM images of iron oxide nanoparticles synthesized by Thermal Decomposition Method 2 at three different magnification. Iron Precursor:  $\text{Fe}(\text{acac})_3$ , solvent: benzyl ether, reducing agent: Oleylamine.

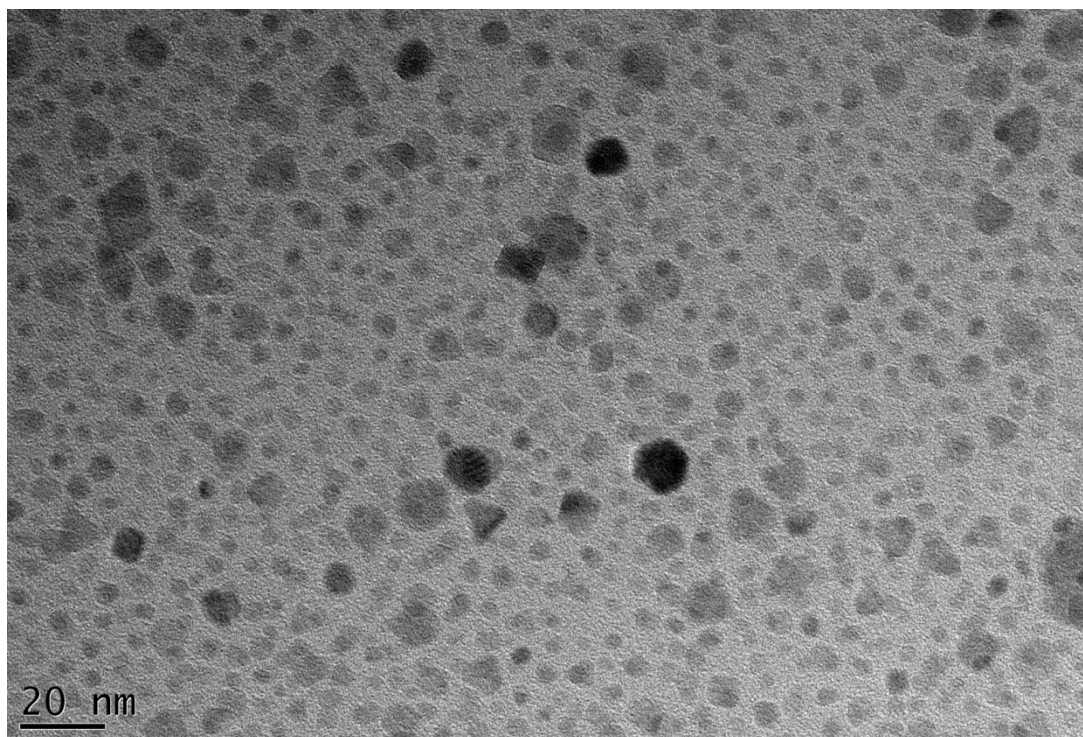
As can be seen from Figure 19, particles synthesized by Method 2 are very uniform in size. Due to the steric repulsions of the surface bonded oleylamine chains, nanoparticles are isolated one from another and the shape of the nanoparticles is nearly spherical.



**Figure 20** TEM images of iron oxide nanoparticles synthesized by thermal decomposition Method 2

From the TEM image, randomly 30 particles were selected. The number-length (arithmetic) mean size ( $D[1,0]$ ) and standard deviations of the iron oxide nanoparticles were calculated as  $5.5 \pm 0.4$  nm. These results indicated that Method 2 in which excess oleylamine was used as an alternative reducing agent instead of an expensive 1,2-hexadecanediol is an efficient and economic alternative to Method 1. Therefore this new method was adopted for the synthesis of the iron oxide nanoparticles.

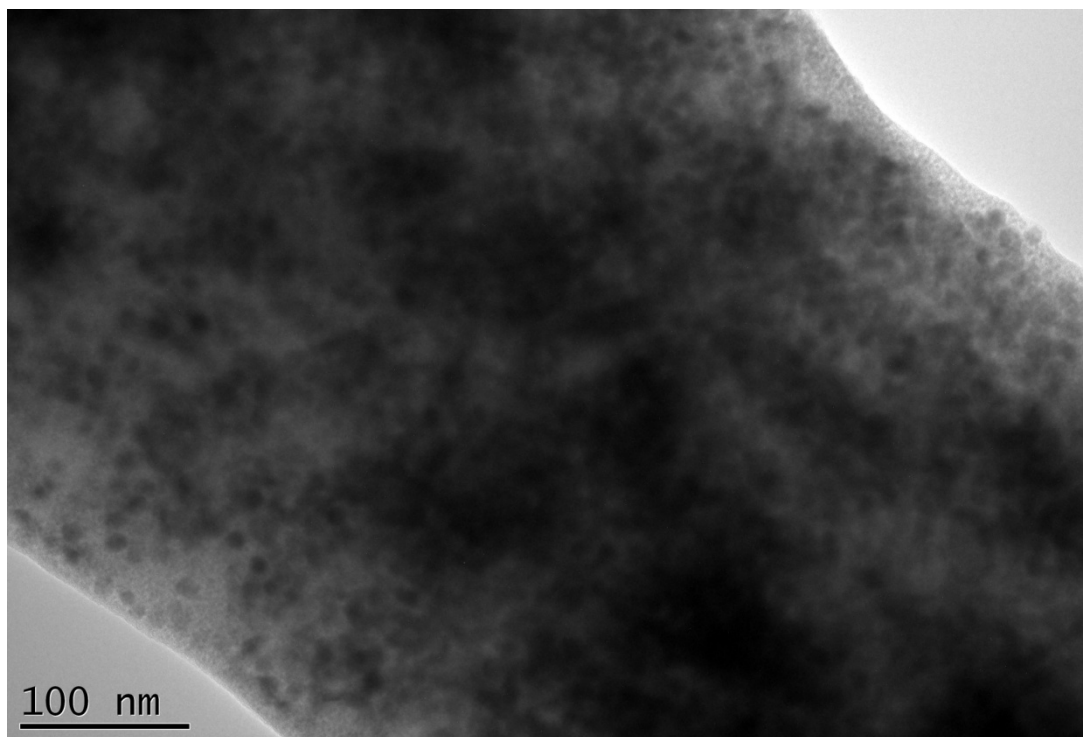
As stated in the previous paragraphs the conditions during the synthesis of the iron oxide particles are very fragile. If the temperature and duration of the decomposition temperature and the rate of the heating were not adjusted properly the nanoparticles may not be stable and they formed large agglomerates (see Figure 18-a) or though they are still in the form of nanoliquid but their homogeneity in terms of shape and size were disturbed. For example, in Method 1 the optimized reflux time was 30 min. The reflux time was extended to 60 min instead of 30 min. The TEM image of the particles obtained under this circumstance is depicted in Figure 21.



**Figure 21** TEM images of iron oxide nanoparticles synthesized by Thermal Decomposition Method 1. Iron Precursor:  $\text{Fe}(\text{acac})_3$ , solvent: benzyl ether, reducing agent: 1,2-hexadecanediol. Reflux time was 60 min. instead of 30 min

As can be seen from Figure 21, the iron oxide nanoparticles were not monodisperse and spherical shape.

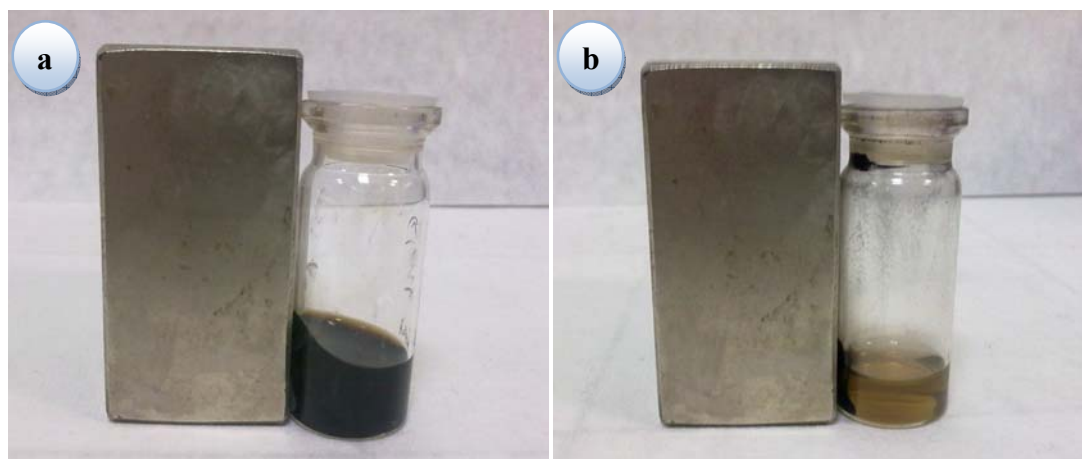
In thermal decomposition method, due to the usage of large amount of oleic acid, precipitation and washing process were also very important parts. It was difficult to remove of oleic acid from the reaction medium. Because of this 5 washing cycles with ethanol were applied. However as can be seen in Figure 22, there was a cloud over the particles, as a result, it was not possible to obtain clear images of the particles [84].



**Figure 22** TEM image of iron oxide nanoparticles synthesized by thermal decomposition method 2 washed once with ethanol.

### 3.1.1 Magnetic Properties of Synthesized Magnetite Nanoparticles

The magnetic properties of the particles will be investigated using VSM (Vibrational sample magnetometer). Particles having size of about 6 nm are expected to show superparamagnetic behavior, which is desired for biological studies. The behavior of the iron oxide nanoparticles dispersed in hexane under a magnetic field is shown in Figure 23. As can be seen from Figure 23-a, in case of the stable iron oxide suspension, the iron oxide particles are attracted to the magnet and the particles climbed to the wall of the container next to the magnet. Figure 23-b shows the influence of the magnetic field on the heavily agglomerated iron oxide particles. As the iron oxide nanoparticles formed large agglomerates, they were attracted strongly to the magnet and a clear solution was formed in a 10 seconds. On the other hand due to their small size the magnetic susceptibility of the iron oxide particles in the stable suspension was comparatively small.



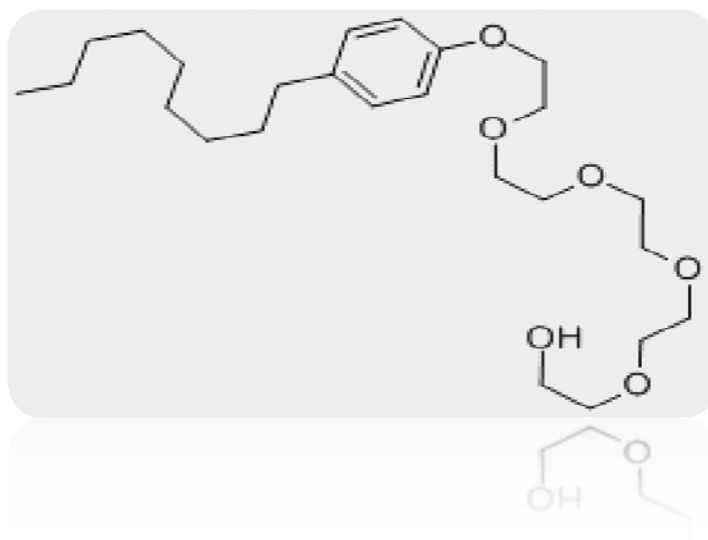
**Figure 23** The behavior of the iron oxide nanoparticles dispersed in hexane under an external magnetic field (1.6 T) applied. a) the stable suspension of iron oxide particles b) large agglomerates of iron oxide particles.

### **3.2 Silica Coating on Iron Oxide Nanoparticles by Reverse Microemulsion Method**

Encapsulation of single nanoparticles with silica shells is advantageous for biological applications, because they can be readily dispersed in aqueous medium and their surfaces can be functionalized easily. Besides silica coating renders the particle nontoxic, and protects the surface of the nanoparticles from oxidation [85].

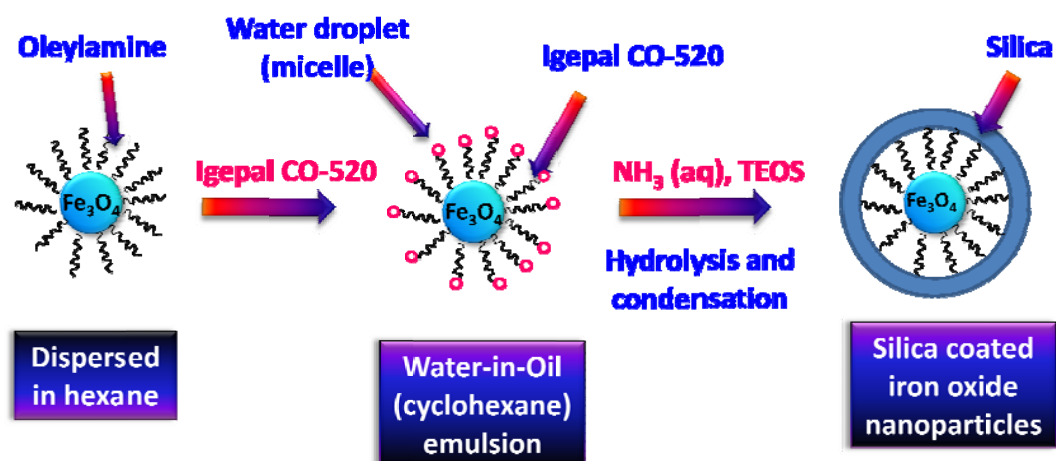
The Stöber method is mainly used for the formation of silica shell around various kind of nanoparticles [86]. However it is not suitable for nanoparticles with nonpolar ligands. Water-in-oil microemulsion (w/o), or inverse microemulsion method is preferred for the silica coating of hydrophobic particles as produced through thermal decomposition method.

As stated in the introduction section, there are two approaches for the explanation of silica shell formation mechanism by inverse microemulsion. The first one which includes phase transfer through surfactant interaction prior to silica coating, without ligand exchange, seemed more probable to us. This involves the interaction of hydrophobic groups of oleylamine around the iron oxide nanoparticles and Igepal CO-520 (Poly(oxyethylene)(5) nonylphenyl ether), a nonionic detergent (Figure 24).



**Figure 24** Chemical formula of Igepal CO-520

Igepal CO-520 could form an “inverse” bilayer around the oleate ligated iron oxides. Water molecules are located in the region of the oxygen groups of Igepal CO-520. On addition of the ammonia catalyst, the silica could grow in the bilayer by hydrolysis and condensation of TEOS, as schematically depicted in Figure 25.



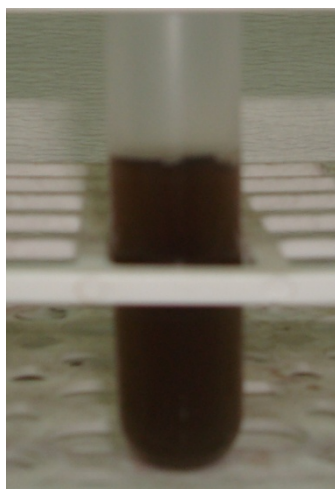
**Figure 25** Synthesis of Silica Coated Iron Oxide Nanoparticles

In the synthesis, cyclohexane served as the continuous phase in which TEOS, Igepal CO-520 and iron oxide particles were dissolved. Subsequently, the ammonia catalyst was added. It was found that the size, monodispersity, and overall quality of the resulting silica coated particles are governed by reaction conditions such as time, concentration of reactants, and speed of stirring. The influence of these conditions was studied systematically and optimum concentrations of Igepal CO-520,  $\text{NH}_3(\text{aq})$  and TEOS were tried to be determined in order to produce controllable silica layer thickness around the particles. Various experimental conditions were tried and the influence of the amount of Igepal CO-520,  $\text{NH}_3(\text{aq})$  and TEOS was studied systematically.

In this study, the synthesis of silica coated particles, having overall size less than 50 nm, highly monodispersed, and non-aggregated single core-shell nanoparticles was our aim. Thus prepared particles should be well-dispersed in water, and these dispersions should be stable for a long time period, therefore following the washing process, the particles were dispersed in water and their photographs were taken after 24 hours. These dispersions were preserved and their appearance were examined on a regular basis. The first sign of the success in the silica coating was



the color of the solution. A reference solution for color comparison was prepared by diluting 467  $\mu\text{l}$  (the amount used in the silica coating process) of uncoated iron oxide nanoparticles to 10 ml with cyclohexane for each batch. A representative reference solution is given in Figure 26.



**Figure 26** Reference solution (Prepared by diluting 467  $\mu\text{l}$  iron oxide nanoparticles to 10 ml cyclohexane).

If the color of the stable aqueous dispersion of silica coated nanoparticle was matched with that of the reference solution, it was considered as a good candidate for further characterization with TEM measurements. The size of the agglomerates was measured using dynamic light scattering method and Polydispersivity index (PDI) which gives information about homogeneity, were calculated. In Table 3, three ranges of polydispersity index values are correlated with the homogeneity of the agglomerates. Throughout this thesis the agglomerate size homogeneity was classified according to Table 3.

**Table 3** The Polydispersivity index values from the DLS method versus particle homogeneity.

<b>Range of Polydispersivity Index Values</b>	<b>Homogeneity of Particles</b>
0.00-0.05	Monodisperse
0.05-0.08	Nearly Monodisperse
0.08-0.7	Mid-range Polydispersivity

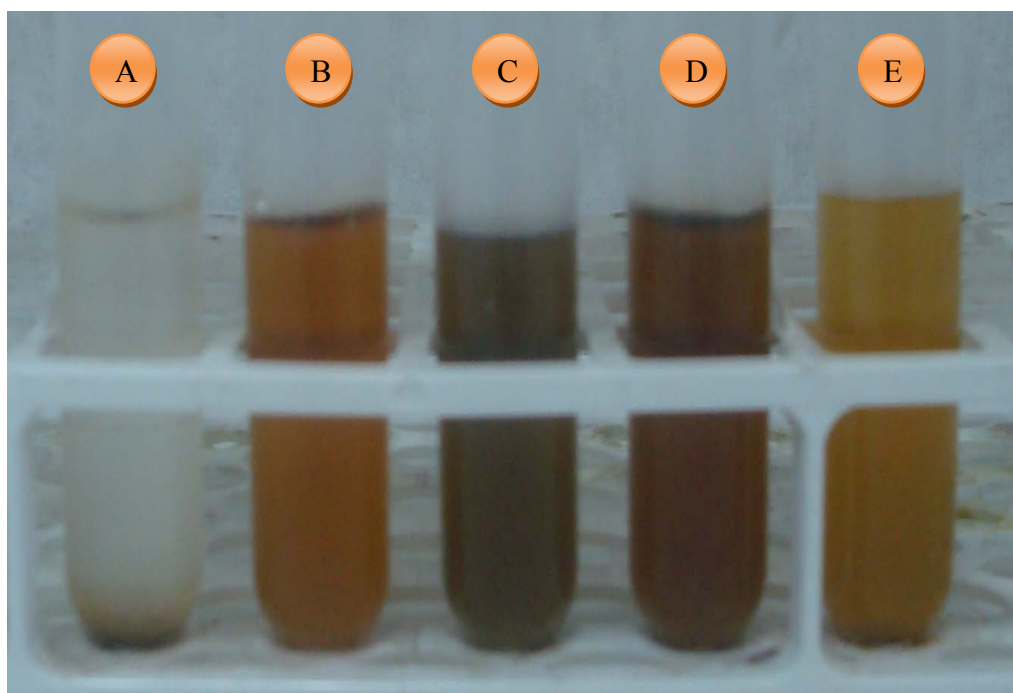
### **3.2.1 Effect of Surfactant on the Silica Coated Iron Oxide Nanoparticles (IGEPAL CO-520)**

Non-ionic surfactant Igepal CO-520 (Poly(oxyethylene)(5) nonylphenyl ether) which acts as a modifier for the reaction environment, was chosen [87]. The Igepal CO-520 lowers the interfacial tension between water and oil, resulting in the formation of a transparent solution [82]. In this section, the volume of Igepal CO-520 was varied in between 500-1500  $\mu$ l, at TEOS volumes of 80 and 100  $\mu$ l, Table 4 and Table 5.

**Table 4** Various surfactant (Igepal CO-520) concentrations used for the synthesis of silica coated iron oxide nanoparticles at low TEOS concentration.

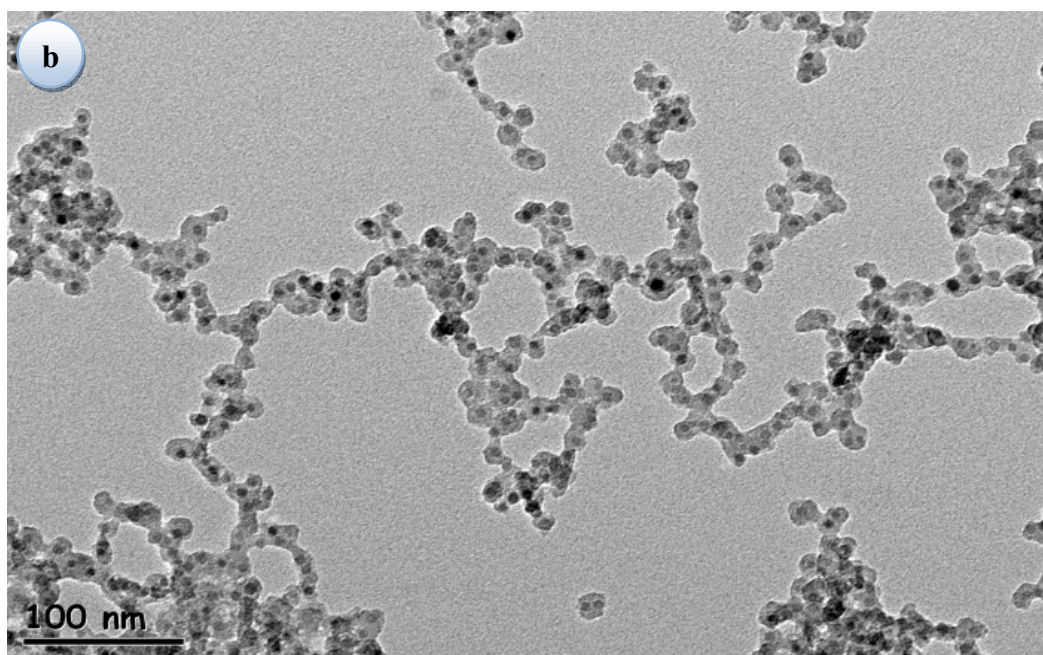
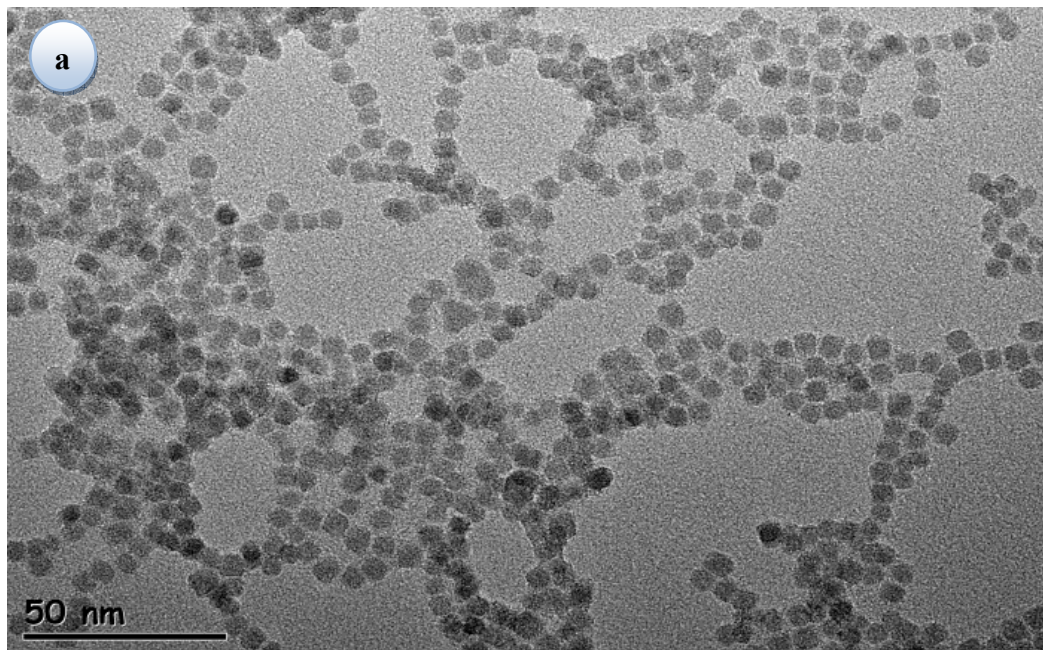
<b>Batches</b>	<b>A</b>	<b>B</b>	<b>C</b>	<b>D</b>	<b>E</b>
<b>Fe<sub>3</sub>O<sub>4</sub></b>	467 $\mu$ l	467 $\mu$ l	467 $\mu$ l	467 $\mu$ l	467 $\mu$ l
<b>Cyclohexane</b>	10 ml	10 ml	10 ml	10 ml	10 ml
<b>Igepal CO-520</b>	<b><u>500 <math>\mu</math>l</u></b>	<b><u>1000 <math>\mu</math>l</u></b>	<b><u>1200 <math>\mu</math>l</u></b>	<b><u>1300 <math>\mu</math>l</u></b>	<b><u>1500 <math>\mu</math>l</u></b>
<b>TEOS</b>	<b><u>80 <math>\mu</math>l</u></b>	<b><u>80 <math>\mu</math>l</u></b>	<b><u>80 <math>\mu</math>l</u></b>	<b><u>80 <math>\mu</math>l</u></b>	<b><u>80 <math>\mu</math>l</u></b>
<b>NH<sub>3</sub>(aq)</b>	150 $\mu$ l	150 $\mu$ l	150 $\mu$ l	150 $\mu$ l	150 $\mu$ l

The appearance of the particles dispersed in water after silica coating process is given in Figure 27. Batch letters (A-E) are also representing these aqueous dispersions of particles.



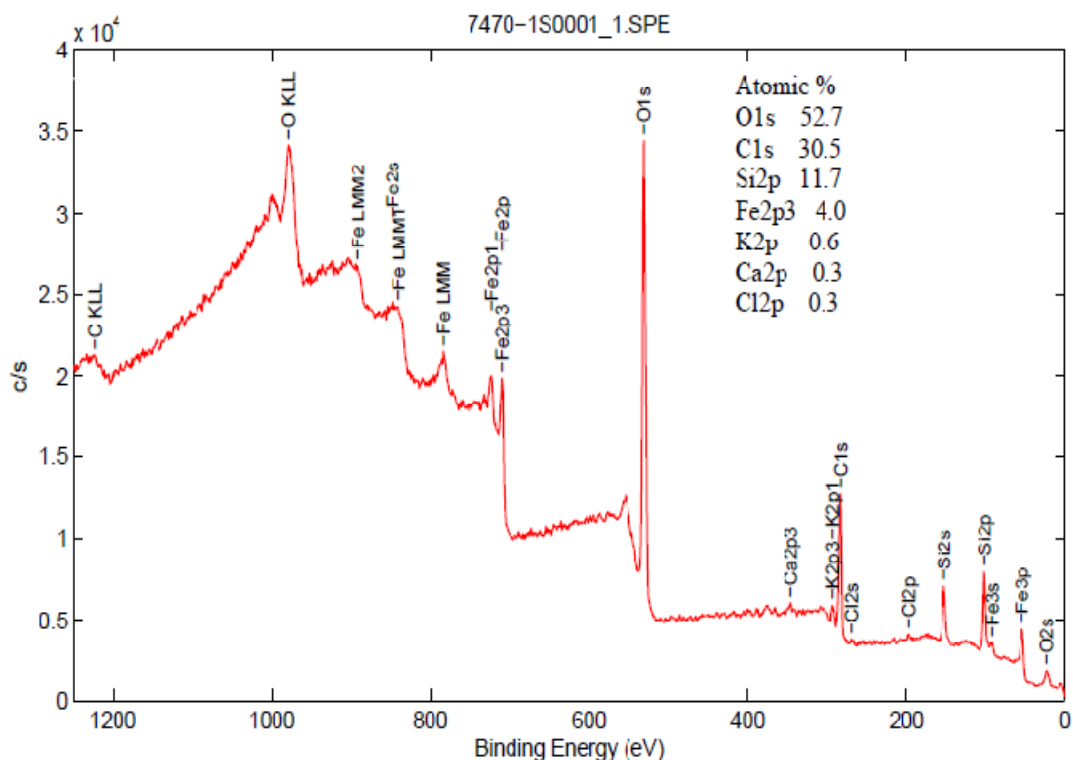
**Figure 27** Photographs of iron oxide nanoparticles following silica coating process. Various amounts of Igepal CO-520 were used at low TEOS concentration, batches A-E a) 500  $\mu\text{l}$  Igepal CO-520; batch A, b) 1000  $\mu\text{l}$  Igepal CO-520; batch B c) 1200  $\mu\text{l}$  Igepal CO-520; batch C d) 1300  $\mu\text{l}$  Igepal CO-520; batch D e) 1500  $\mu\text{l}$  Igepal CO-520; batch E, (80  $\mu\text{l}$  TEOS was used)

As can be seen from Figure 27, when the concentration of the surfactant was changed, the suspensions with various colors were produced. The lowest Igepal CO-520 was used in suspension A, the iron oxide particles were agglomerated in 1 day. In other suspensions, there were no evidence of any significant agglomeration. TEM images of batch B and D were taken and presented in Figure 28.



**Figure 28** TEM images of the silica coated iron oxide nanoparticles prepared using 80  $\mu\text{l}$  TEOS, 150  $\mu\text{l}$   $\text{NH}_3(\text{aq})$  and Igepal CO-520 a) 1000  $\mu\text{l}$  Igepal CO-520; batch B, b) 1300  $\mu\text{l}$  Igepal CO-520; batch D.

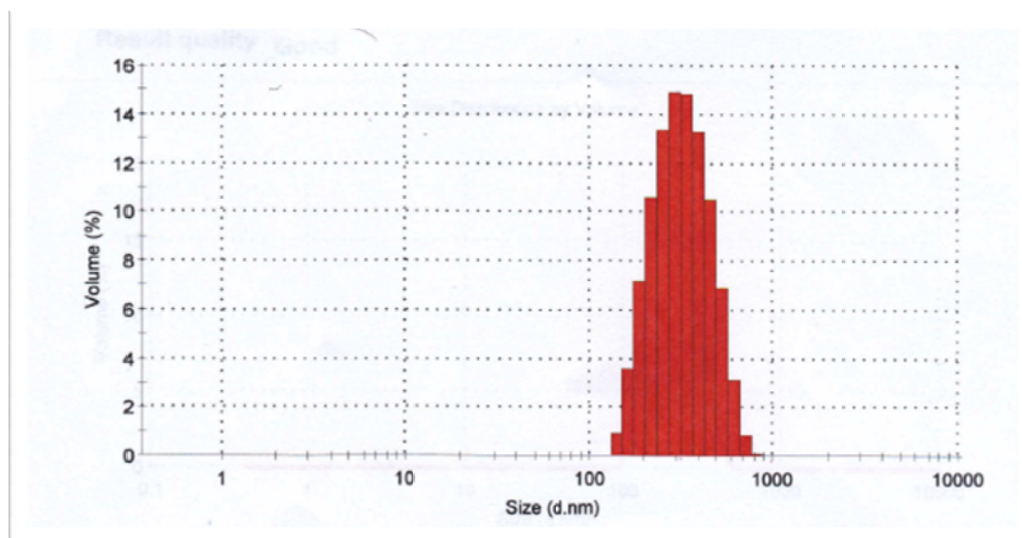
As can be seen in Figure 28-a, when 1000  $\mu\text{l}$  surfactant was used, batch B, the silica layers around particles could not be observed in the TEM image. The size of the nanoparticles after silica coating process was measured as  $6.1 \pm 0.4$  nm. The original size of the iron oxide particles used in this batch was  $5.5 \pm 0.4$  nm. Considering the size difference in between the silica coated ( $6.1 \pm 0.4$  nm) and uncoated iron oxide particles ( $5.5 \pm 0.4$ ) and the stability (5 months) of the aqueous dispersion of the silica coated particles (batch B), it was thought that the iron oxide particles were coated with a very thin layer of silica which might be beyond the resolution limit of TEM (less than 0.2 nm). Therefore another surface technique, XPS, was used to investigate the presence of silica on the surface of the iron oxide particles. XPS spectrum is presented in Figure 29.



**Figure 29** XPS result of silica coated iron oxide nanoparticles of batch B.

As can be seen in the XPS spectrum, the concentration of Si on the surface on the iron oxide particles was 11.7 atomic % suggesting the presence of silica layer on the surface of the iron oxide particles. However, as can be seen in Figure 29, 4.0 atomic % Fe was also observed on the same particles. The presence of Fe can be explained either by the formation of very thin layer of silica (ca 0.2 nm) or partial coating of silica around iron oxide nanoparticles.

The agglomerate size distribution of the silica coated iron oxide nanoparticles were measured for batch B and D. The size distribution of the silica coated iron oxide agglomerates for batch B is shown in Figure 30.



**Figure 30** The agglomerate size distribution of the silica coated iron oxide nanoparticles prepared using 1000  $\mu\text{l}$  Igepal CO-520, 80  $\mu\text{l}$  TEOS and 150  $\mu\text{l}$  of  $\text{NH}_3(\text{aq})$ .



The z-average mean size of the silica coated iron oxide agglomerates for batch B and D were 298 nm and  $196 \pm 8.6$  nm respectively. Although the agglomerate size of the particles in batch D was smaller than that of batch B, they were still very large compared to the primary particle size  $6.1 \pm 0.4$  nm. PDI of batch B and D were calculated as 0.133 and  $0.134 \pm 0.06$  respectively which were corresponding to a mid-range polydisperse agglomerate size distribution.

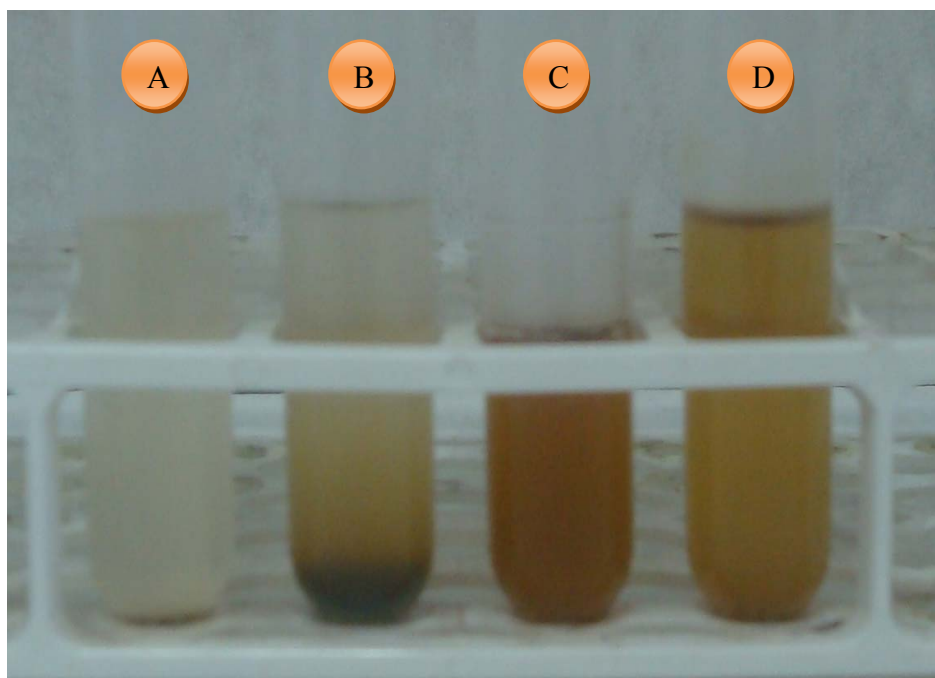
The surfactant concentration was varied again in the range of 500-1500  $\mu$ l at high TEOS concentration (100  $\mu$ l TEOS). The volume of other materials were held constant ( 150  $\mu$ l of  $\text{NH}_3(\text{aq})$ , 467  $\mu$ l of a iron oxide stock solution).

**Table 5** Various surfactant (Igepal CO-520) concentrations used for the synthesis of silica coated iron oxide nanoparticles at high TEOS concentration.

<b>Batches</b>	<b>A</b>	<b>B</b>	<b>C</b>	<b>D</b>
<b><math>\text{Fe}_3\text{O}_4</math></b>	467 $\mu$ l	467 $\mu$ l	467 $\mu$ l	467 $\mu$ l
<b>Cyclohexane</b>	10 ml	10 ml	10 ml	10 ml
<b>Igepal CO-520</b>	<b><u>500 <math>\mu</math>l</u></b>	<b><u>1000 <math>\mu</math>l</u></b>	<b><u>1300 <math>\mu</math>l</u></b>	<b><u>1500 <math>\mu</math>l</u></b>
<b>TEOS</b>	<b><u>100 <math>\mu</math>l</u></b>	<b><u>100 <math>\mu</math>l</u></b>	<b><u>100 <math>\mu</math>l</u></b>	<b><u>100 <math>\mu</math>l</u></b>
<b><math>\text{NH}_3(\text{aq})</math></b>	150 $\mu$ l	150 $\mu$ l	150 $\mu$ l	150 $\mu$ l

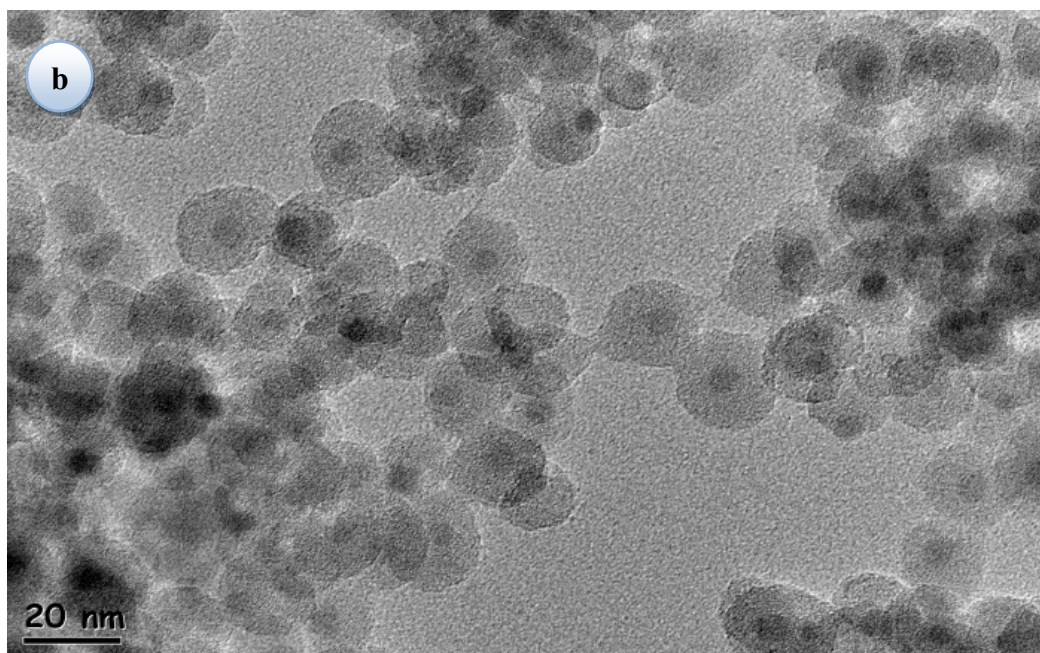
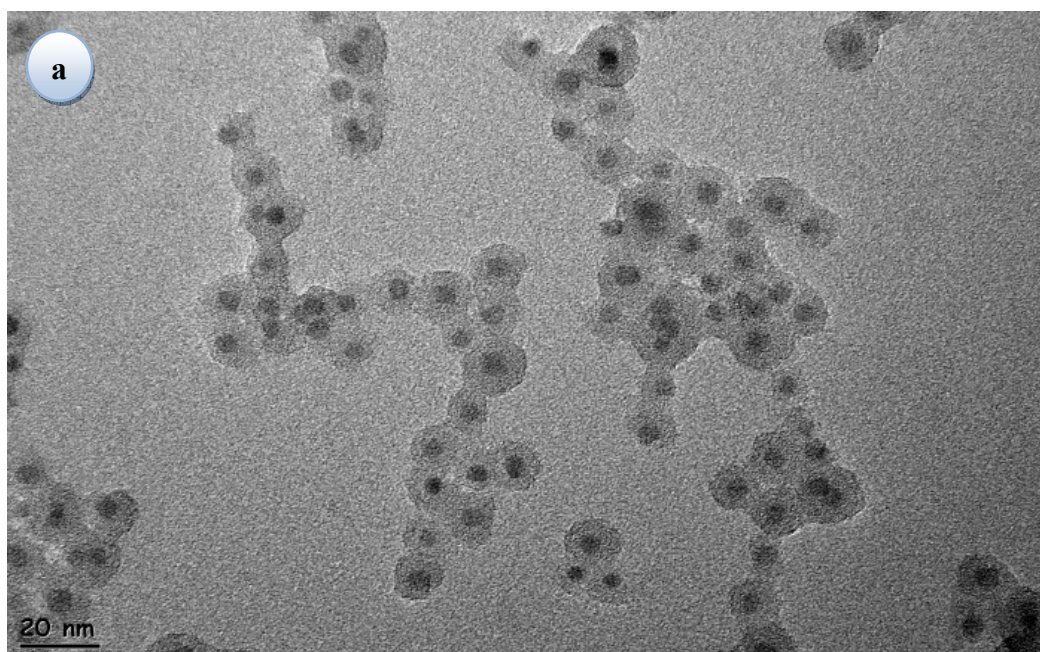


The appearance of the particles dispersed in water after silica coating process is given in Figure 31.



**Figure 31** Photographs of iron oxide nanoparticles following silica coating process. Various amounts of Igepal CO-520 were used at high TEOS concentration, batches A-D a) 500  $\mu\text{l}$  Igepal CO-520; batch A, b) 1000  $\mu\text{l}$  Igepal CO-520; batch B c) 1300  $\mu\text{l}$  Igepal CO-520; batch C d) 1500  $\mu\text{l}$  Igepal CO-520; batch D (100  $\mu\text{l}$  TEOS was used)

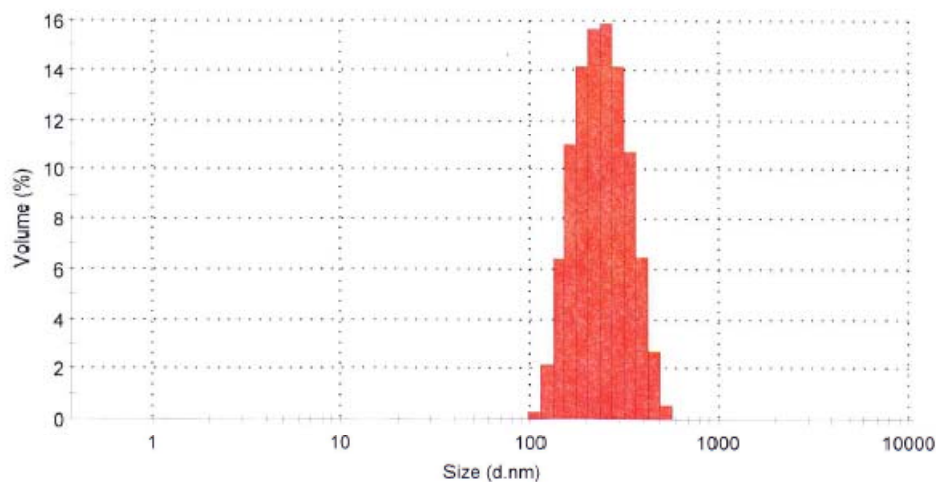
As can be seen from Figure 31, the aqueous dispersions obtained through batches of A and B were precipitated after 1 day, whereas batches C and D were stable. The TEM images of these stable dispersions, batch C and D, were taken and presented in Figure 32.



**Figure 32** TEM images of iron oxide nanoparticles following silica coating process. Various amounts of Igepal CO-520 were used at high TEOS concentration and 150  $\mu\text{l}$   $\text{NH}_3(\text{aq})$  a) 1300  $\mu\text{l}$  Igepal CO-520; batch C b) 1500  $\mu\text{l}$  Igepal CO-520; batch D. (100  $\mu\text{l}$  TEOS was used)

As can be seen from the TEM images (see Figure 32-a and b), when 1300 and 1500  $\mu\text{l}$  Igepal CO-520 were used during the coating process, the batches C and D, all the iron oxide nanoparticles were coated with silica. The thickness of the coated silica layer was measured by taking the difference in the number-length mean sizes of the silica coated iron oxide nanoparticles and iron oxide nanoparticles. For the batch C (see Table 5), the primary particle size of the iron oxide nanoparticles was measured as  $5.5 \pm 0.4$  nm and the silica coated nanoparticles were measured as  $13.5 \pm 0.7$  nm from Figure 32-a. Therefore, the thickness of the silica layer coated on the iron oxide nanoparticles was calculated as  $3.9 \pm 0.3$  nm. For the batch D, the primary particle size of iron oxide nanoparticles was measured as approximately  $6.3 \pm 0.8$  nm and the silica coated nanoparticles were measured as approximately  $19 \pm 1$  nm from Figure 32-b. Therefore, the thickness of silica layer coated on the iron oxide nanoparticles was estimated as approximately  $6.4 \pm 0.5$  nm. The silica layer thickness was increased from  $3.9 \pm 0.3$  nm to  $6.4 \pm 0.5$  nm when the volume of Igepal CO-520 used in coating was increased from 1300 to 1500  $\mu\text{l}$ . These results have shown that the surfactant Igepal CO-520 plays an important role for the thickness of the silica shell around the iron oxide nanoparticles. Another important point was that the particle separation was getting better when the thickness of silica layer on the iron oxide particles was increased.

The agglomerate size distribution of batches C and D were measured and distribution for batch C is presented in Figure 33.



**Figure 33** The agglomerate size distribution of the silica coated iron oxide nanoparticles prepared using 1300  $\mu\text{l}$  Igepal CO-520, 100  $\mu\text{l}$  TEOS and 150  $\mu\text{l}$  of  $\text{NH}_3(\text{aq})$ .

The z-average mean sizes of the silica coated iron oxide agglomerates prepared using 1300 and 1500  $\mu\text{l}$  Igepal CO-520 were about 282 nm and  $289 \pm 10$  nm respectively. These observations have shown that the amount of the surfactant did not influence the agglomerate size of the silica coated iron oxide nanoparticles. PDI of the silica coated iron oxide nanoparticles prepared using 1300  $\mu\text{l}$  and 1500  $\mu\text{l}$  Igepal CO-520 together with 100  $\mu\text{l}$  TEOS were calculated as 0.048 and  $0.165 \pm 0.030$  respectively. According to the PDI values, the batch C was classified as a monodisperse, whereas, the batch D was considered as a mid-range polydisperse agglomerate.

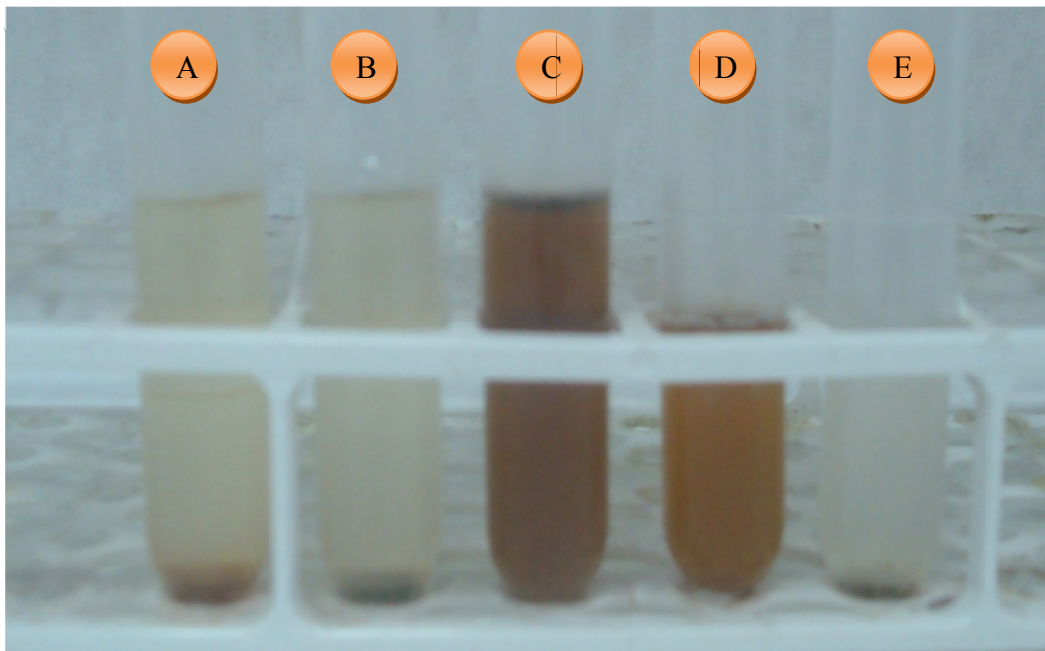
### 3.2.2 Effect of TEOS Solution on Silica Coated Iron Oxide Nanoparticles

The influence of the TEOS concentration on the thickness of the silica coating was observed in the previous section. In order to investigate this parameter extensively, the volume of TEOS used in the silica coating was varied in the range of 60 to 120  $\mu\text{l}$ , while the other parameters were held constant (1300  $\mu\text{l}$  of Igepal CO-520, 150  $\mu\text{l}$  of  $\text{NH}_3(\text{aq})$ , 467  $\mu\text{l}$  of the iron oxide stock solution, (see Table 6).

**Table 6** Various concentrations of TEOS used for the preparation of silica coated iron oxide particles.

Batches	A	B	C	D	E
$\text{Fe}_3\text{O}_4$	467 $\mu\text{l}$	467 $\mu\text{l}$	467 $\mu\text{l}$	467 $\mu\text{l}$	467 $\mu\text{l}$
Cyclohexane	10 ml	10 ml	10 ml	10 ml	10 ml
Igepal CO-520	1300 $\mu\text{l}$	1300 $\mu\text{l}$	1300 $\mu\text{l}$	1300 $\mu\text{l}$	1300 $\mu\text{l}$
TEOS	<u>60 <math>\mu\text{l}</math></u>	<u>70 <math>\mu\text{l}</math></u>	<u>80 <math>\mu\text{l}</math></u>	<u>100 <math>\mu\text{l}</math></u>	<u>120 <math>\mu\text{l}</math></u>
$\text{NH}_3(\text{aq})$	150 $\mu\text{l}$	150 $\mu\text{l}$	150 $\mu\text{l}$	150 $\mu\text{l}$	150 $\mu\text{l}$

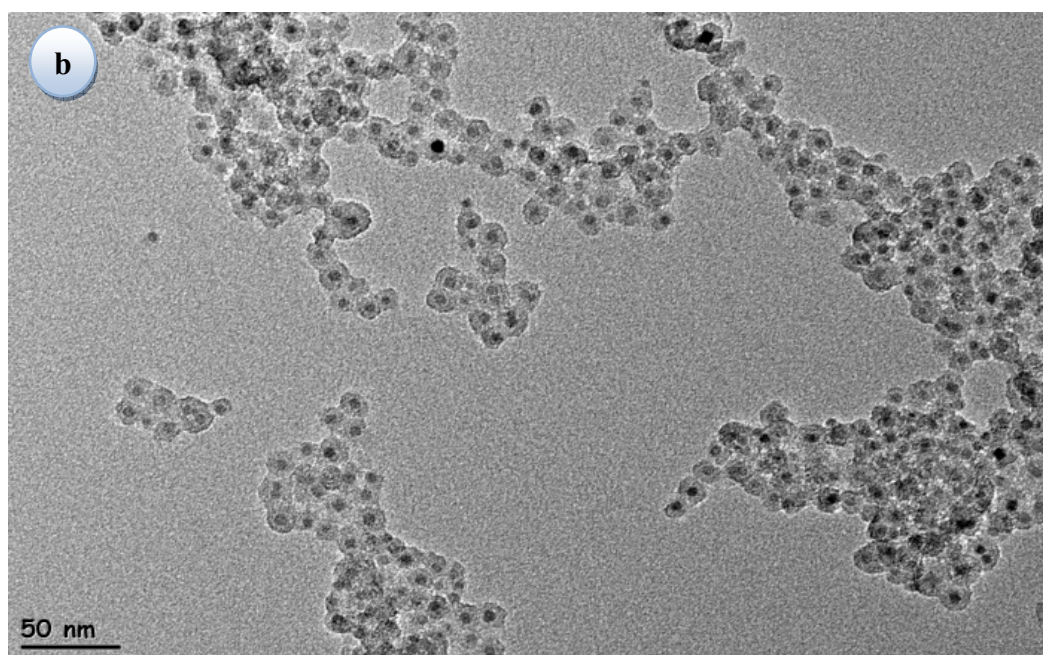
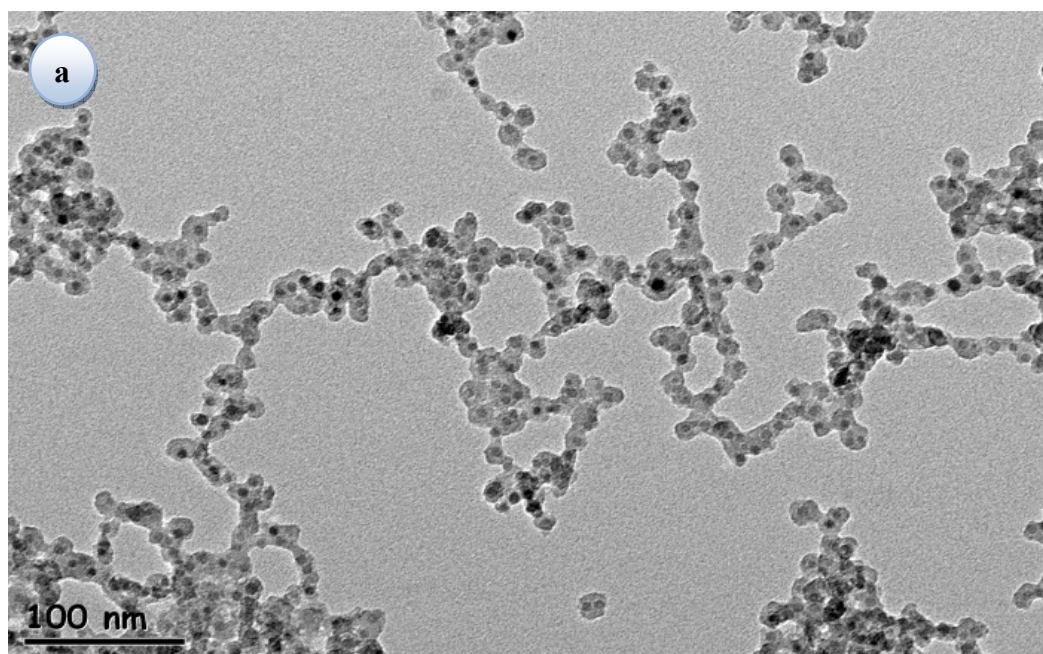
The appearance of the particles dispersed in water after silica coating process is given in Figure 34. Batch letters (A-E) are also representing these aqueous dispersions of the particles.



**Figure 34** Photographs of iron oxide nanoparticles following the silica coating process in which various amounts of TEOS were used. a) 60  $\mu\text{l}$  TEOS; batch A, b) 70  $\mu\text{l}$  TEOS; batch B c) 80  $\mu\text{l}$  TEOS; batch C d) 100  $\mu\text{l}$  TEOS; batch D e) 120  $\mu\text{l}$  TEOS; batch E. Volume of Igepal CO-520 was 1300  $\mu\text{l}$ .

As can be seen from Figure 34, the particles were settled down after 1 day for batches A, B and E. The batches C and D which were prepared using 80  $\mu\text{l}$  and 100  $\mu\text{l}$  of TEOS respectively were stable after waiting 2 months. The TEM images of the batches C and D were taken and presented in Figure 35.



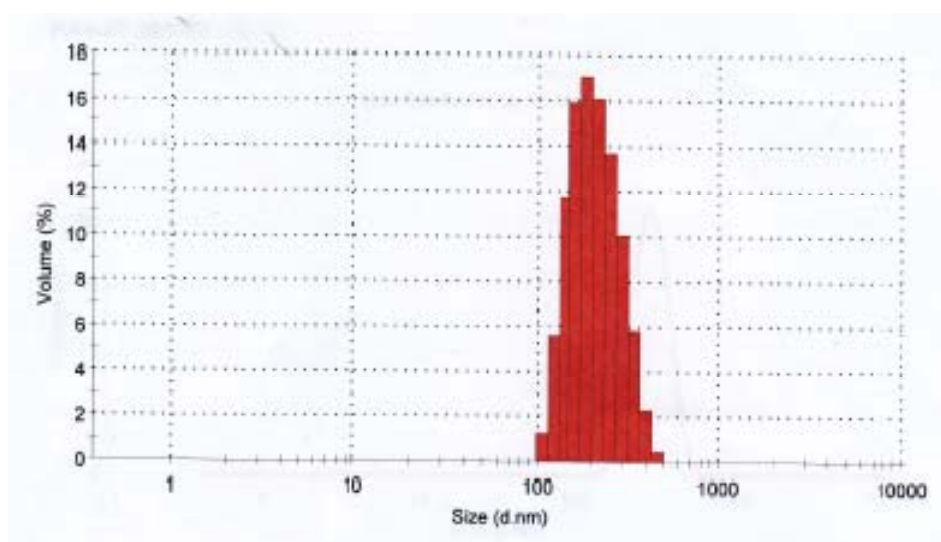


**Figure 35** TEM images of the silica coated iron oxide nanoparticles prepared using 1300  $\mu\text{l}$  Igepal CO-520 and various amounts of TEOS a) 80  $\mu\text{l}$  TEOS; batch C, b) 100  $\mu\text{l}$  TEOS; batch D was used.

It was observed that when 80  $\mu\text{l}$  and 100  $\mu\text{l}$  TEOS were used, all the iron oxide nanoparticles were coated with silica (see Figure 35), but these silica coated iron oxide nanoparticles were again in the form of agglomerates.

From the TEM images, the primary particle sizes of the silica coated iron oxide nanoparticles were measured as  $13.9 \pm 1.3 \text{ nm}$  and  $13.5 \pm 0.7 \text{ nm}$  and the thickness of the silica layers around them were estimated as approximately  $3.72 \pm 0.80 \text{ nm}$  and  $3.9 \pm 0.3 \text{ nm}$  for the batches C and D, respectively (Figure 35). These observations have shown that at the specified (1300  $\mu\text{l}$ ) Igepal CO-520 concentration, the increase in TEOS concentration did not influence the silica shell thickness significantly.

The size of the agglomerates for the batches A, C, D, E was measured. The agglomerate size distribution of the silica coated iron oxide nanoparticles for the batch E is given in Figure 36.



**Figure 36** The agglomerate size distribution of the silica coated iron oxide nanoparticles prepared using 1300  $\mu\text{l}$  Igepal CO-520, 120  $\mu\text{l}$  TEOS and 150  $\mu\text{l}$  of  $\text{NH}_3(\text{aq})$ , batch E.



The z-average mean size of the silica coated iron oxide agglomerates for the batch E (120  $\mu$ l TEOS) was measured about  $206 \pm 7$  nm. The z-average mean agglomerate sizes of the silica coated iron oxide nanoparticles prepared using 100, 80 and 60  $\mu$ l TEOS ( Batches D, C, A) were determined as 282 nm,  $196 \pm 9$  nm and  $223 \pm 5$  nm respectively. Although the values were close to each other, the smallest agglomerate size was obtained for the Batch C (80  $\mu$ l).

PDI values of silica coated iron oxide nanoparticles which was prepared using 60  $\mu$ l, 80  $\mu$ l 100  $\mu$ l and 200  $\mu$ l TEOS (batches A, C, D, E) were calculated as  $0.09 \pm 0.04$ ,  $0.134 \pm 0.100$ ,  $0.048$  and  $0.135 \pm 0.030$ , respectively. According to these results monodisperse agglomerate size distribution was observed only for the batch D (100  $\mu$ l TEOS). The rest were considered as mid-range polydisperse agglomerates.

### **3.2.3 Effect of Ammonia Solution on Silica Coated Iron Oxide Nanoparticles**

Ammonia is a catalyst which accelerates the hydrolysis of TEOS proportionally. In order to obtain monodisperse particle, rapid hydrolysis is preferred [82].

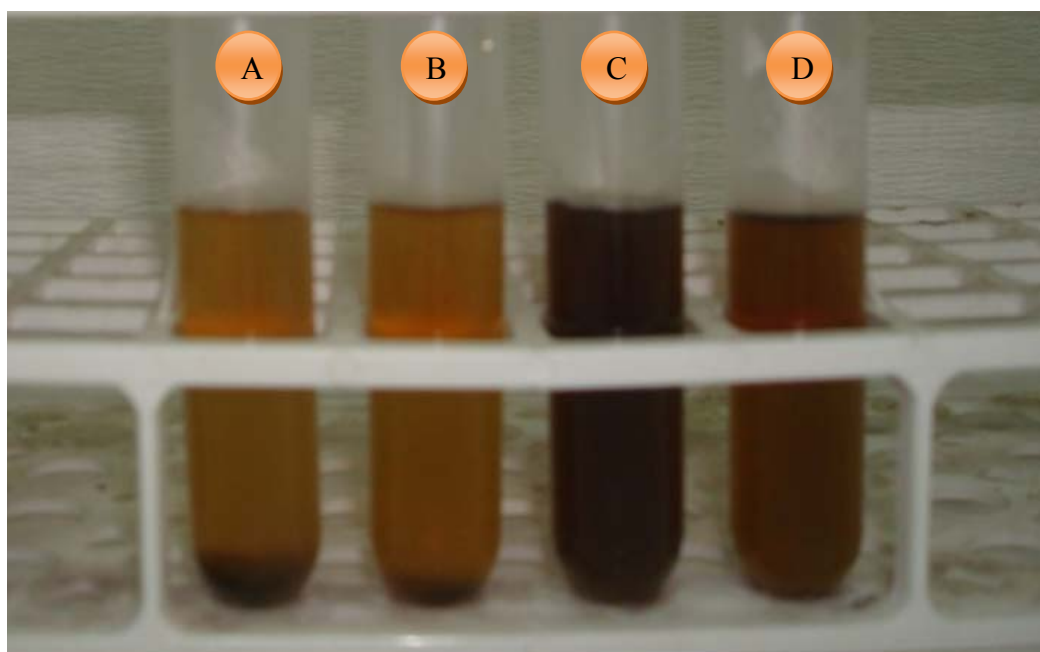
$\text{NH}_3(\text{aq})$  was added dropwise because when the larger volumes of  $\text{NH}_3(\text{aq})$  was added, irreversible precipitation of the core nanoparticles was occurred.

As can be seen from the Table 7 and Table 8, the amount of  $\text{NH}_3(\text{aq})$  was varied changed from 75 to 200  $\mu$ l, at two different TEOS concentrations (80 and 100  $\mu$ l of TEOS were used) when the amount of other materials was held constant (1300  $\mu$ l of Igepal CO-520, 467  $\mu$ l of the iron oxide stock solution).

**Table 7** Various concentrations of NH<sub>3</sub>(aq) used for the preparation of silica coated iron oxide particles at low TEOS concentration.

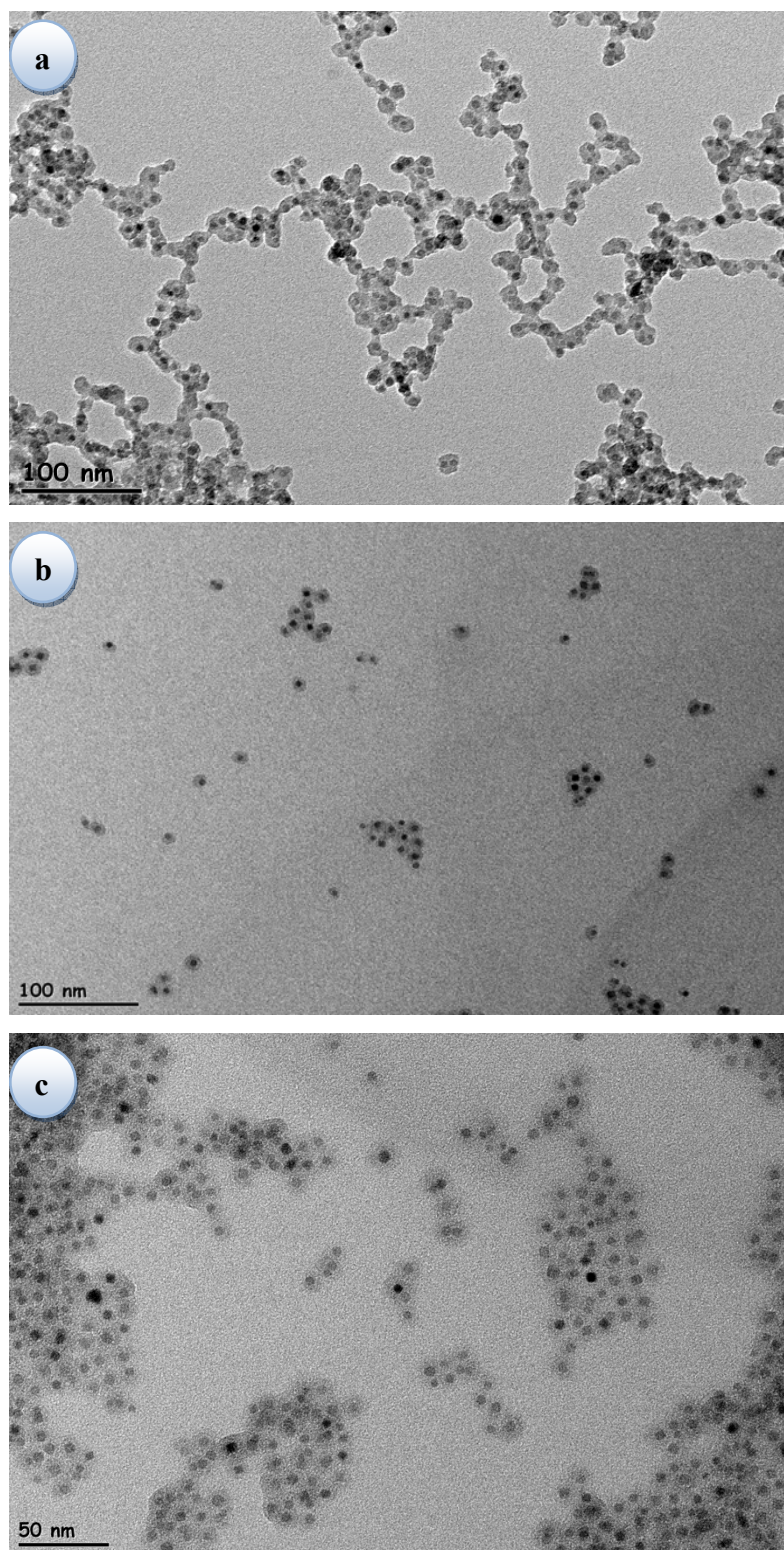
<b>Batches</b>	<b>A</b>	<b>B</b>	<b>C</b>	<b>D</b>
<b>Fe<sub>3</sub>O<sub>4</sub></b>	467 µl	467 µl	467 µl	467 µl
<b>Cyclohexane</b>	10 ml	10 ml	10 ml	10 ml
<b>Igepal CO-520</b>	1300 µl	1300 µl	1300 µl	1300 µl
<b>TEOS</b>	<b><u>80 µl</u></b>	<b><u>80 µl</u></b>	<b><u>80 µl</u></b>	<b><u>80 µl</u></b>
<b>NH<sub>3</sub>(aq)</b>	<b><u>75 µl</u></b>	<b><u>100 µl</u></b>	<b><u>150 µl</u></b>	<b><u>200 µl</u></b>

The appearance of the particles dispersed in water after silica coating process is given in Figure 37. Batch letters (A-D) are also representing these aqueous dispersions of iron oxide particles.



**Figure 37** Photographs of iron oxide nanoparticles following the silica coating process in which various amounts of  $\text{NH}_4\text{OH}$  a)  $75 \mu\text{l}$   $\text{NH}_4\text{OH}$ ; batch A b)  $100 \mu\text{l}$   $\text{NH}_4\text{OH}$ ; batch B c)  $150 \mu\text{l}$   $\text{NH}_3(\text{aq})$ ; batch C d)  $200 \mu\text{l}$  Igepal  $\text{NH}_4\text{OH}$ ; batch D ( $80 \mu\text{l}$  TEOS and  $1300 \mu\text{l}$  Igepal CO-520 was used)

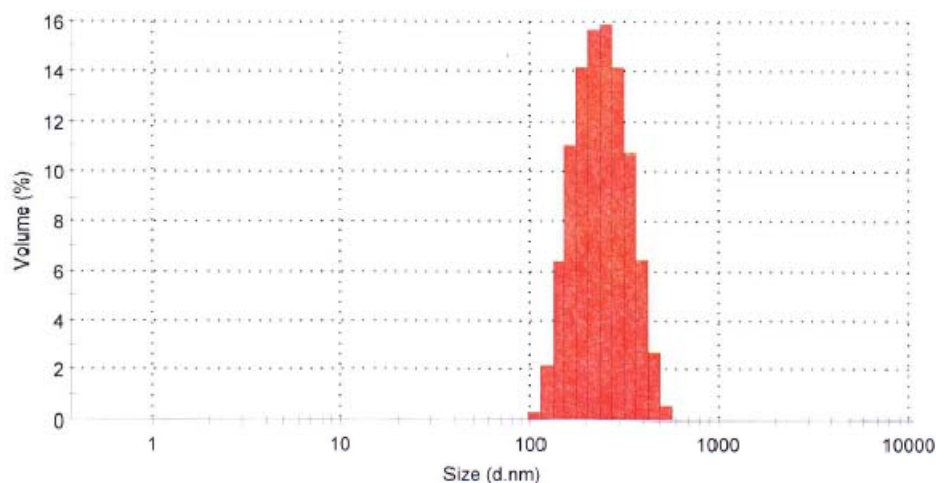
As can be seen from Figure 37, the aqueous dispersions of the batches A and B were not stable after waiting 1 day. The dispersions of the batches C and D, which were prepared by using  $150 \mu\text{l}$  and  $200 \mu\text{l}$   $\text{NH}_3(\text{aq})$  respectively, were stable. The TEM images of these stable suspensions, the batches C and D, were taken and presented in Figure 38.



**Figure 38** TEM images of iron oxide nanoparticles prepared using 1300  $\mu\text{l}$  Igepal CO-520, 80  $\mu\text{l}$  TEOS and two different amounts of  $\text{NH}_3(\text{aq})$  a) 150  $\mu\text{l}$   $\text{NH}_3(\text{aq})$ ; batch C, b) and c) 200  $\mu\text{l}$   $\text{NH}_4\text{OH}$ ; batch D.

From TEM images, the primary particle size of the silica coated iron oxide nanoparticles was measured as  $13.9 \pm 1.3$  nm and the thickness of the silica layers was determined as  $3.72 \pm 0.80$  nm which was prepared using 150  $\mu$ l  $\text{NH}_3(\text{aq})$  (Figure 38-a). The primary particle size of silica coated iron oxide nanoparticles prepared using 200  $\mu$ l  $\text{NH}_3(\text{aq})$  was measured as  $14.5 \pm 1.8$  nm and the thickness of the silica layer was determined as  $4.3 \pm 0.7$  nm (see Figure 38-b,c). Although there is a slight increase in the silica shell thickness when the amount of  $\text{NH}_3(\text{aq})$  was changed from 150 to 200  $\mu$ l at the specified conditions (1300  $\mu$ l of Igepal CO-520, 80  $\mu$ l of TEOS, 467  $\mu$ l of the iron oxide stock solution), the change is not significant.

The size of the agglomerates in the batches C, D, was measured. The agglomerate size distribution of the silica coated iron oxide nanoparticles for batch D (200  $\mu$ L  $\text{NH}_3(\text{aq})$ ) is given in Figure 39.



**Figure 39** The agglomerate size distribution of the silica coated iron oxide nanoparticles prepared using 1300  $\mu$ l Igepal CO-520, 80  $\mu$ l TEOS and 200  $\mu$ l of  $\text{NH}_3(\text{aq})$ , batch D.

The z-average mean agglomerate size of the silica coated iron oxide particles in the batch D was about 234 nm. The agglomerate size of the silica coated iron oxide particles which was prepared using 150  $\mu\text{L}$   $\text{NH}_3(\text{aq})$ , the batch C, was about  $196 \pm 9$  nm (Figure 38-a). Although the primary particle size of the silica coated iron oxide agglomerates as observed in the TEM image of batch D (Figure 38-b,c), was very small, the agglomerate size of the iron oxide particles in the batches C and D, were around 200 nm.

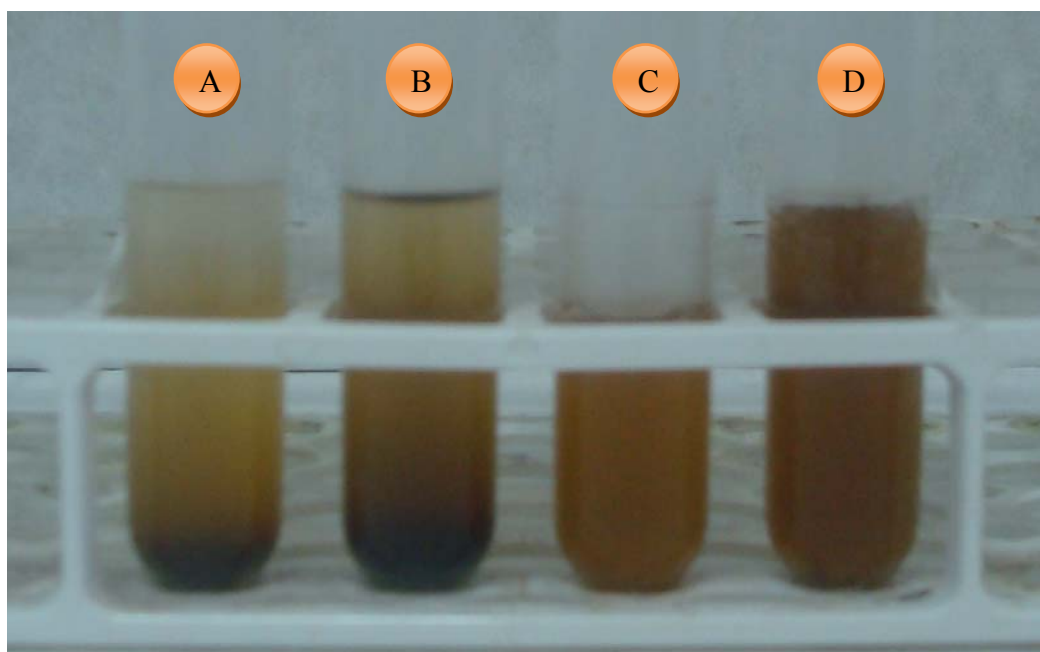
PDI of silica coated iron oxide nanoparticles which were prepared using 150  $\mu\text{l}$  and 200  $\mu\text{l}$   $\text{NH}_3(\text{aq})$  at low TEOS concentration (80  $\mu\text{l}$  TEOS), were calculated as  $0.134 \pm 0.100$  and 0.066, respectively. These results indicated that, nearly monodisperse agglomerate size distribution was obtained for the suspension D and mid-range polydisperse agglomerate size distribution was obtained for the suspension C.

This time the effect of  $\text{NH}_3(\text{aq})$  concentration on the thickness of the silica shell was investigated at high concentration of TEOS. Thus, the amount of  $\text{NH}_3(\text{aq})$  was varied in the range of 75 to 200  $\mu\text{l}$  in the presence of 100  $\mu\text{l}$  TEOS. The amount of the other materials was held constant (see Table 8).

**Table 8** Various NH<sub>3</sub>(aq) concentrations used for the synthesis of the silica coated iron oxide nanoparticles at high TEOS concentration.

<b>Batches</b>	<b>A</b>	<b>B</b>	<b>C</b>	<b>D</b>
<b>Fe<sub>3</sub>O<sub>4</sub></b>	467 μl	467 μl	467 μl	467 μl
<b>Cyclohexane</b>	10 ml	10 ml	10 ml	10 ml
<b>Igepal CO-520</b>	1300 μl	1300 μl	1300 μl	1300 μl
<b>TEOS</b>	<u>100 μl</u>	<u>100 μl</u>	<u>100 μl</u>	<u>100 μl</u>
<b>NH<sub>3</sub>(aq)</b>	<u>75 μl</u>	<u>100 μl</u>	<u>150 μl</u>	<u>200 μl</u>

The appearance of the particles dispersed in water after silica coating process is given in Figure 40. Batch letters (A-D) are also representing these aqueous dispersions of particles.



**Figure 40** Photographs of SiO<sub>2</sub> coated Fe<sub>3</sub>O<sub>4</sub> nanoparticle suspensions prepared using different amounts of NH<sub>3</sub>(aq) a) 75  $\mu$ l NH<sub>3</sub>(aq); batch A b) 100  $\mu$ l NH<sub>3</sub>(aq); batch B c) 150  $\mu$ l NH<sub>3</sub>(aq); batch C d) 200  $\mu$ l NH<sub>3</sub>(aq); batch D (100  $\mu$ l TEOS and 1300  $\mu$ l Igepal CO-520 was used)

As can be seen in Figure 40, only the dispersions of the batch C and D which were prepared using 150  $\mu$ l and 200  $\mu$ l NH<sub>3</sub>(aq), respectively and 100  $\mu$ l TEOS, were stable. The z-average mean agglomerate size of the silica coated iron oxide particles in the batch C was about 282 nm. The agglomerate size of the silica coated iron oxide particles which was prepared using 200  $\mu$ L NH<sub>3</sub>(aq), the batch D, was about  $224 \pm 10$  nm.

PDI of silica coated iron oxide nanoparticles which was prepared by 150  $\mu$ l and 200  $\mu$ l NH<sub>3</sub>(aq), when 100  $\mu$ l TEOS was used, was calculated as 0.048 and  $0.121 \pm 0.050$ , respectively. Thus, monodisperse agglomerate size distribution was obtained for the batch C and a mid-range polydisperse agglomerate size distribution was obtained for the batch D.



## CHAPTER 4

### CONCLUSIONS

In this thesis, thermal decomposition method was used for the synthesis of monodispersed and small sized iron oxide nanoparticles. An economical way of preparation of the iron oxide nanoparticles without using external expensive reducing reagent, 1,2-hexadecanediol, was tried. The iron oxide nanoparticles thus prepared were characterized using the transmission electron microscopy (TEM). From the TEM images, the primary particle size of iron oxide nanoparticles were calculated as approximately  $5.5 \pm 0.4$  nm and homogeneous size distribution was clearly seen.

The iron oxide nanoparticles were coated with thin silica shell via reverse microemulsion method. The influence of the amounts of Igepal CO-520,  $\text{NH}_3(\text{aq})$  and TEOS was studied systematically and their amounts were optimized to yield monodisperse and well defined particles. TEM images were used to follow the silica thickness around particles. The most important parameter controlling the thickness of the silica layer was the amount of Igepal CO-520. Silica layer thickness was increased from  $3.9 \pm 0.3$  nm to  $6.4 \pm 0.5$  nm when the volume of Igepal CO-520 was increased from 1300 to 1500  $\mu\text{l}$ . The contribution of the other parameters, such as the amounts of  $\text{NH}_3(\text{aq})$  and TEOS, were not significant. Agglomerate sizes of the particles obtained at various experimental conditions were measured using the dynamic light scattering method and the polydispersity index (PDI), which gives information about homogeneity, were calculated. The z-average mean sizes of the silica coated iron oxide agglomerates prepared between 195 and 298 nm. These observations have shown that experimental conditions did not influence the agglomerate size of the silica coated iron oxide nanoparticles. According to the PDI values, the silica coated iron oxide agglomerates prepared

using 1300  $\mu\text{l}$  Igepal CO-520, 100  $\mu\text{l}$  TEOS and 150  $\mu\text{l}$   $\text{NH}_3(\text{aq})$  was classified as a monodisperse, whereas, the other batches were considered as a mid-range polydisperse agglomerates. For further studies, we will try to solve the irreversible agglomeration problems of silica coated iron oxide nanoparticles.

## REFERENCES

1. L. Williams, (2007), "Nanotechnology Demystified", United States of America, McGraw-Hill.
2. R. Feynman, (1991), *Science* 254, 1300-1301.
3. O. Salata, (2004), *Journal of Nanobiotechnology* 2, 1-6.
4. J. Mongillo, (2007), "Nanotechnology 101", London, Greenwood Press.
5. E. S. Papazoglou, A. Parthasarathy, (2007), "BioNanotechnology", Philadelphia, Morgan & Claypool.
6. D. H. H. Sevcics, *Approaches to Safe Nanotechnology*, (2009), *Approaches to Safe Nanotechnology*, DHHS (NIOSH).
7. I. Brigger, C. Dubernet, P. Couvreur, (2002), *Adv. Drug Deliv. Rev.* 54, 631-651.
8. R. Nagarajan, T. A. Hatton, (2008), "Nanoparticles: Synthesis, Stabilization, Passivation and Functionalization", Washington, DC, American Chemical Society.
9. Y.-W. Jun, J.-W. Seo, J. Cheon, (2008), *Accounts of Chemical Research* 41, 179-189.
10. A.-H. Lu, E. L. Salabas, F. Schüth, (2007), *Angew. Chem. Int. Ed.* 46, 1222-1244.
11. D. Portet, B. Denizot, E. Rump, J. J. Lejeune, P. Jallet, (2001), *J. Colloid Interface Sci.* 238, 37.
12. P. Tartaj, M. d. P. Morales, S. Veintemillas-Verdaguer, T. Gonzalez-Carreno, C. J. Serna, (2003), *J. Phys. D: Appl. Phys.* 36, 182-197.

13. A. Jordan, R. Scholz, K. Maier-Hauff, M. Johannsen, P. Wust, J. Nadobny, H. Schirra, H. Schmidt, S. Deger, S. Loening, W. Lanksch, R. Felix, (2001), *J. Magn. Magn. Mater* 225, 118.
14. C. C. Berry, A. S. G. Curtis, (2003), *J. Phys. D: Appl. Phys.* 36, 198-206.
15. Q. A. Pankhurst, J. Connolly, S. K. Jones, J. Dobson, (2003), *J. Phys. D Appl. Phys.* 36, 167-181.
16. S. Mornet, S. Vasseur, F. Grasset, E. Duguet, (2004), *J. Mater. Chem.* 2161.
17. W. Cai, J. Wan, (2007), *J. Colloid and Interface Sci.* 305, 366-370.
18. L. R, (1990), *Science* 249, 1527.
19. N. Yahya, (2010), "Carbon and Oxide Nanostructures Synthesis, Characterisation and Applications", Malaysia, Springer.
20. A. Ito, M. Shinkai, H. Honda, T. Kobayashi, (2005), *J. Biosci. Bioeng.* 100, 1-11.
21. I. Safarik, M. Safarikova, (2002), *Monats. Chem.* 133, 737.
22. R. Weissleder, D. D. Stark, B. L. Engelstad, B. R. Bacon, C. C. Compton, D. L. White, P. Jacobs, J. Lewis, (1989), *American Journal of Roentgenology* 152, 167-173.
23. S. F. Chin, S. C. Pang, C. H. Tan, (2011), *J. Mater. Environ. Sci.* 2 3, 299-302.
24. R. M. Cornell, U. Schwertmann, (2003), "The Iron Oxides: Structures, Properties, Reactions, Occurences and Uses", New York, Wiley-VCH.
25. W. Wu, Q. He, C. Jiang, (2008), *Nanoscale Res Lett* 3, 397-415.
26. J. P. Jakubovics, (1994), "Magnetism and Magnetic Materials", Cambridge, The Institute of Materials, Cambridge.

27. M. Ozaki, E. Matijevic, (1985), *J. Colloid Interface Sci.* 107, 199.
28. T. Gonzalez-Carreno, A. Mifsud, C. J. Serna, J. M. Palacios, (1991), *Mater. Chem. Phys.* 27, 287.
29. R. F. Ziolo, E. P. Giannelis, B. A. Weinstein, M. P. O'Horo, B. N. Ganguly, V. Mehrotra, M. W. Russell, D. R. Huffman, (1992), *Science* 257, 219.
30. A. S. Teja, P.-Y. Koh, (2009), *Prog. Cryst. Growth Characterisation Mater* 55, 22–45.
31. S. P. Gubin, Y. A. Koksharov, G. B. Khomutov, G. Y. Yurkov, (2005), *Russian Chemical Reviews* 74, 489-520.
32. S. Qu, H. Yang, D. Ren, S. Kan, G. Zou, D. Li, M. Li, (1999), *J. Colloid and Interface Sci.* 215, 190-192.
33. C. Sun, J. S. H. Lee, M. Zhang, (2008), *Advanced Drug Delivery Reviews* 60, 1252-1265.
34. D. Halliday, R. Resnick, J. Walker, (1997), "Fundamentals of Physics: Extended", New York, John Wiley & Sons, Inc.
35. N. A. Spaldn, (2003), "Magnetic Materials: Fundamentals and Device Applications", Cambridge University Press.
36. D. William, J. Callister, (2000), "Material Science and Engineering: An Introduction", New York, John Wiley & Sons.
37. R. C. O. Handley, (2000), "Modern Magnetic Materials: Principles and Applications", New York, Wiley & Sons.
38. C. Kittel, (1986), "Introduction to Solid State Physics", New York, John Wiley & Sons, Inc.
39. N. Poudyal, 2005, "Synthesis and Characterization of Magnetic Nanoparticles", Master of the Science in Physics, Texas at Arlington, Texas.

40. A. H. Morrish, (2001), "The Physical Principles of Magnetism", New York, IEEE Press.
41. K. J. Klabunde, (2001), "Nanoscale Materials in Chemistry", New Jersey, John & Sons, Inc.
42. M. A. Zalich, 2005, "Physical Properties of Magnetic Macromolecule-Metal and Macromolecule-Metal Oxide Nanoparticle Complexes", Doctor of Philosophy In Chemistry, State University, Blacksburg, Virginia.
43. B. Bonnemain, (1998), *J. Drug Target* 6, 167-174.
44. Y. X. Wang, S. M. Hussain, G. P. Krestin, (2001), *Eur. Radiol* 11, 2319–2331.
45. S. R. Dave, X. Gao, (2009 ), *Nanobiotechnoly* 1, 583–609.
46. M. Faraji, Y. Yamini, M. Rezaee, (2010), *J. Iran. Chem. Soc.* 7, 1-37.
47. M. Mohapatra, S. Anand, (2010), *IJEST* 2, 127-146.
48. G. L. Messing, S. Zhang, G. V. Jayanthi, (1993), *J. Am. Ceram. Soc.* 76, 2707.
49. J. Park, K. An, Y. Hwang, J.-G. Park, H.-J. Noh, J.-Y. Kim, J.-H. Park, N.-M. Hwang, T. Hyeon, (2004), *Nat. Mater.* 3, 891.
50. S. Sun, H. Zeng, D. B. Robinson, S. Raoux, P. M. Rice, S. X. Wang, G. Li, (2004), *J. Am. Chem. Soc.* 126, 273-279.
51. F. X. Redl, C. T. Black, G. C. Papaefthymiou, R. L. Sandstrom, M. Yin, H. Zeng, C. B. Murray, S. P. O'Brien, (2004), *J. Am. Chem. Soc.* 126, 14583.
52. J. Rockenberger, E. C. Scher, A. P. Alivisatos, (1999), *J. Am. Chem. Soc.* 11595.
53. D. Farrell, S. A. Majetich, J. P. Wilcoxon, (2003), *J. Phys. Chem. B* 107, 11022.

54. J. Park, E. Lee, N. M. Hwang, M. Kang, S. C. Kim, Y. Hwang, J. G. Park, H. J. Noh, J. Y. Kim, J. H. Park, T. A. Hyeon, (2005), *Chem. Int. Ed.* 44, 2872.
55. S. Sun, H. Zeng, (2002), *J. Am. Chem. Soc.* 124, 8204.
56. N. R. Jana, Y. Chen, X. Peng, (2004), *Chem. Mater.* 16, 3931.
57. A. C. S. Samia, K. Hyzer, J. A. Schlueter, C.-J. Qin, J. S. Jiang, S. D. Bader, X.-M. Lin, (2005), *J. Am. Chem. Soc.* 127, 4126.
58. Y. Li, M. Afzaal, P. O'Brien, (2006), *J. Mater. Chem.* 16, 2175.
59. B. Denizot, G. Tanguy, F. Hindre, E. Rump, J. J. Lejeune, P. Jallet, (1999), *J. Colloid Interface Sci.* 209, 66.
60. J. L. Lyon, D. A. Fleming, M. B. Stone, P. Schiffer, M. E. Williams, (2004), *Nano Lett.* 4, 719.
61. Q. Liu, J. A. Finch, R. Egerton, (1998), *Chem. Mater.* 10, 3936.
62. A. Ulman, (1996), *Chem. Rev.* 1533.
63. A.-L. Morel, S. I. Nikitenko, K. Gionnet, A. Wattiaux, J. Lai-Kee-Him, C. Labrugere, B. Chevalier, G. Deleris, C. Petibois, A. Brisson, M. Simonoff, (2008), *ACS Nano* 2, 847-856.
64. Y.-H. Deng, C.-C. Wang, J.-H. Hu, W.-L. Yang, S.-K. Fu, (2005), *Colloids and Surfaces A: Physicochem. Eng. Aspects* 262, 87-93.
65. G. A. V. Ewijk, G. J. Vroege, A. P. Philipse, (1991), *J. Magn. Magn. Mater.* 201, 31.
66. C. Chaneac, E. Tronc, J. P. Jolivet, (1995), *Nanostruct. Mater.* 6, 715-718.
67. G. M. Chow, K. E. Gonsalves, M. R. Zachariah, R. D. Shull, B. K. McMillin, P. Biswas, (1996), "Nanotechnology: Molecularly Designed Materials", Washington, DC, ACS Symposium Series, 622.

68. C. R. Vestal, J. Zhang, (2003), *Nanoletters* 3, 1739-1743.
69. S. Santra, R. Tapeç, N. Theodoropoulou, J. Dobson, A. Hebard, W. Tan, (2001), *Langmuir* 17, 2900.
70. P. Tartaj, J. S. Carlos, (2003), *J. Am. Chem. Soc.* 125, 15754.
71. S. K. Young, (2006), *Material Matters* 1.3, 8.
72. C. Solans, P. Izquierdo, J. Nolla, N. Azemar, M. J. G.-. Celma, (2005), *Curr. Opin. Colloid Interface Sci.* 10, 102.
73. D. K. Yi, S. S. Lee, G. C. Papaefthymiou, J. Y. Ying, (2006), *Chem. Mater.* 18, 614-619.
74. U. Jeong, X. Teng, Y. Wang, H. Yang, Y. Xia, ( 2007), *Adv. Mater.* 19, 33–60.
75. C. Vogt, M. S. Toprak, M. Muhammed, S. Laurent, J.-L. Bridot, R. N. Müller, (2010), *J Nanopart Res* 12, 1137–1147.
76. M. Darbandi, R. Thomann, T. Nann, (2005), *Chem. Mater.* 17, 5720-5725.
77. M. Zhang, B. L. Cushing, C. J. O'Connor, (2007), *Nanotechnology* 19, 085601-085605.
78. C. Vogt, M. S. Toprak, M. Muhammed, S. Laurent, J.-L. Bridot, R. N. Müller, (2010), *J Nanopart Res* 12, 1137–1147.
79. A. Rawle, (2002), *Advances in Colour Science and Technology* 5, 1-12.
80. A. G. Roca, J. F. Marco, M. d. P. Morales, C. J. Serna, (2007), *J. Phys. Chem. C* 111, 18577-18584.
81. Z. Xu, C. Shen, Y. Hou, H. Gao, S. Sun, (2009), *Chem. Mater.* 21, 1778–1780.



82. M. Darbandi, 2007, "Silica coated nanocomposites", Albert-Ludwigs-University, Germany.
83. A. M. Pereira, C. Pereira, A. S. Silva, D. S. Schmool, C. Freire, J.-M. Grenèche, J. P. Araújo, (2011), *J. Appl. Phys.* 109, 114319-114323.
84. Z. Tatlıcı, 2010, "Preparation And Characterization Of Magnetite Nanoparticles By Thermal Decomposition Method For Their Potential Use In Tumor Imaging", M.S thesis, Middle East Technical University, Ankara, Türkiye.
85. S. Rahmani, 2011, "Design of Coated Magnetic Iron-Oxide Nanogels for Drug Delivery Systems", University of Waterloo, Waterloo, Ontario, Canada.
86. J. Lodhia, G. Mandarano, N. Ferris, P. Eu, S. Cowell, (2010), *Biomed Imaging Interv. J.* 6, e12.
87. V. T. Son, L. V. Phong, M. N. Islam, T. Q. Hung, S. Kim, J.-H. Jeong, C. Kim, J.-R. Jeong, (2010), *J. Mag.* 15, 112-115.